



PII S0016-7037(00)00408-7

^{206}Pb – ^{230}Th – ^{234}U – ^{238}U and ^{207}Pb – ^{235}U geochronology of Quaternary opal, Yucca Mountain, Nevada

LEONID A. NEYMARK,^{1,*} YURI V. AMELIN,² and JAMES B. PACES¹

¹U.S. Geological Survey, Denver Federal Center, Denver, Colorado 80225, USA

²Jack Satterly Geochronology Laboratory, Royal Ontario Museum, Toronto, Ontario, M5S 2C6, Canada

(Received July 13, 1999; accepted in revised form March 29, 2000)

Abstract—U–Th–Pb isotopic systems have been studied in submillimeter-thick outermost layers of Quaternary opal occurring in calcite–silica fracture and cavity coatings within Tertiary tuffs at Yucca Mountain, Nevada, USA. These coatings preserve a record of paleohydrologic conditions at this site, which is being evaluated as a potential high-level nuclear waste repository. The opal precipitated from groundwater is variably enriched in ^{234}U (measured $^{234}\text{U}/^{238}\text{U}$ activity ratio 1.124–6.179) and has high U (30–313 ppm), low Th (0.008–3.7 ppm), and low common Pb concentrations (measured $^{206}\text{Pb}/^{204}\text{Pb}$ up to 11,370). It has been demonstrated that the laboratory acid treatment used in this study to clean sample surfaces and to remove adherent calcite, did not disturb U–Th–Pb isotopic systems in opal.

The opal ages calculated from $^{206}\text{Pb}^*/^{238}\text{U}$ and $^{207}\text{Pb}^*/^{235}\text{U}$ ratios display strong reverse discordance because of excess radiogenic $^{206}\text{Pb}^*$ derived from the elevated initial ^{234}U . The data are best interpreted using projections of a new four-dimensional concordia diagram defined by $^{206}\text{Pb}^*/^{238}\text{U}$, $^{207}\text{Pb}^*/^{235}\text{U}$, $^{234}\text{U}/^{238}\text{U}_{\text{activity}}$, and $^{230}\text{Th}/^{238}\text{U}_{\text{activity}}$. Ages and initial $^{234}\text{U}/^{238}\text{U}$ activity ratios have been calculated using different projections of this diagram and tested for concordance. The data are discordant, that is observed $^{207}\text{Pb}^*/^{235}\text{U}$ ages of 170 ± 32 (2σ) to 1772 ± 40 ka are systematically older than $^{230}\text{Th}/\text{U}$ ages of 34.1 ± 0.6 to 452 ± 32 ka.

The age discordance is not a result of migration of uranium and its decay products under the open system conditions, but a consequence of noninstantaneous growth of opal. Combined U–Pb and $^{230}\text{Th}/\text{U}$ ages support the model of slow mineral deposition at the rates of millimeters per million years resulting in layering on a scale too fine for mechanical sampling. In this case, U–Pb ages provide more accurate estimates of the average age for mixed multiage samples than $^{230}\text{Th}/\text{U}$ ages, because ages based on shorter-lived isotopes are nonlinearly biased by younger mineral additions.

Use of the combined U–Th–Pb technique to date Yucca Mountain Quaternary opals significantly extends the age range beyond that of the $^{230}\text{Th}/\text{U}$ dating method and shows that selected fracture pathways in the unsaturated zone felsic tuffs of Yucca Mountain have been active throughout the Quaternary. *Copyright © 2000 Elsevier Science Ltd*

1. INTRODUCTION

Yucca Mountain, Nevada, is under investigation as a potential site for a high-level radioactive waste repository (U.S. Department of Energy, 1988). Because groundwater constitutes the most likely medium for transporting radionuclides from the proposed repository to the accessible environment, determining the nature and rate of water movement through the unsaturated (vadose) zone (UZ) at Yucca Mountain is a critical task for assessing the future performance of a nuclear waste repository. The lack of long-term direct measurements of infiltration requires proxy indicators of water movements through the unsaturated zone to estimate historic infiltration patterns. A reliable chronology of low-temperature fracture- and cavity-coating minerals precipitated from percolating groundwater is needed to better understand the paleohydrology of the site. Previously obtained $^{230}\text{Th}/\text{U}$ ages for outermost layers of low-temperature subsurface fracture- and cavity-coating opal and calcite were systematically older than ^{14}C ages for calcite (Neymark and Paces, 1996, 2000; Paces et al., 1996, 1998a; Neymark et al., 1998b). On the basis of the textures of minerals and the age

data, a depositional model was proposed (Neymark and Paces, 2000) where very thin layers were added more or less continuously on a scale finer than sampling techniques can resolve. The model assumes that analyzed samples represent mixtures of materials of different ages and predicts age discordance between isotopic systems with different half-lives.

To obtain further constraints on the history of the fracture- and cavity-coating minerals, we developed a combined U–Th–Pb dating technique allowing the measurement of different parent–daughter isotope systems in the same material. The advantage of the U–Pb dating method is that unlike $^{230}\text{Th}/\text{U}$ and ^{14}C techniques, it allows age estimates from different Pb/U isotope ratios that can be tested for concordance and used as an internal criterion of closed system behavior. In addition, the combined U–Th–Pb technique extends the maximum age limit of datable material (>1 Ma) beyond that of $^{230}\text{Th}/\text{U}$ dating method (<500 ka), which is desirable for better understanding the long-term hydrologic history of Yucca Mountain.

Opal samples were selected for this study because they have U contents that are three to five orders of magnitude higher than coexisting calcite (Paces et al., 1998a) and, thus, are more conducive to detailed microsample U–Th–Pb geochronologic

*Author to whom correspondence should be addressed (lneymark@usgs.gov).

studies. Additional benefits are provided by high $^{238}\text{U}/^{232}\text{Th}$ and $^{238}\text{U}/^{204}\text{Pb}$ ratios and low initial ^{230}Th and ^{204}Pb concentrations caused by differences in solubility of U, Th, and Pb in oxidizing groundwater (Gascoyne, 1992). Previous attempts to use opal as a U–Pb geochronometer had demonstrated its potential for dating Miocene and Pliocene geologic events (Ludwig et al., 1980; Zielinski, 1982). In these studies mineral ages were calculated from $^{207}\text{Pb}/^{235}\text{U}$, whereas $^{206}\text{Pb}/^{238}\text{U}$ ratios were only used to estimate initial $^{234}\text{U}/^{238}\text{U}$ values assuming closed system conditions.

The combination of the U–Pb and U-series geochronometers provides new opportunities for dating complex young geologic systems as long as the problem of severe initial radioactive disequilibrium is addressed. The problem of initial excess or deficit of intermediate daughter nuclides in the $^{238}\text{U}/^{206}\text{Pb}$ and $^{235}\text{U}/^{207}\text{Pb}$ decay chains, caused by elemental fractionation during crystallization of Th- and U-enriched minerals in magmatic systems, and their impact on precise U–Pb geochronology was discussed in a series of papers (Mattinson, 1973; Schärer, 1984; Parrish, 1990; Barth et al., 1994; Oberli et al., 1996; Amelin and Zaitsev, 1997). Because minerals were too old to observe radioactive disequilibrium directly, in all these studies an initial disequilibrium was assumed to explain discordant U–Pb ages. To our knowledge, to date the only study attempted to combine U–Pb and U-series dating techniques was done on a U-rich speleothem of Quaternary age (Richards et al., 1998) and gave a concordant $^{207}\text{Pb}/^{235}\text{U}$ isochron and $^{230}\text{Th}/\text{U}$ age. Geologically young Yucca Mountain opals precipitated from water with large U/Th and U/Pb ratios enable direct observation of radioactive disequilibrium and its impact on U–Pb data.

This paper presents results of a combined U–Pb and U-series geochronologic study of Quaternary opal in the Tertiary tuffs at Yucca Mountain, Nevada, and describes new dating techniques with U–Pb systems containing excesses of ^{234}U and ^{230}Th with measured $^{234}\text{U}/^{238}\text{U}$ and $^{230}\text{Th}/^{238}\text{U}$ activity ratios appreciably exceeding unity.

2. GEOLOGIC SETTING AND SAMPLES

Yucca Mountain is located within the southwestern Nevada volcanic field (Christiansen et al., 1977) and is composed of a 1 to 3 km thick sequence of faulted felsic volcanic rocks formed around 13 Ma (Sawyer et al., 1994). The present-day arid climate and 400 to 600 m thick unsaturated zone are considered to be positive attributes of the site (Winograd, 1981), which is being evaluated as a potential national underground high-level radioactive waste repository. Faulting and fracturing formed a network that may facilitate fluid movement within the otherwise low permeability welded tuff. Submillimeter to 5 cm thick secondary calcite and opal deposits coat-selected fracture footwalls and floors of lithophysal cavities (primary voids formed during cooling of tuffs).

Subsurface opal at Yucca Mountain forms submillimeter-thick clear, solid hemispheres, botryoidal masses, or thin sheets coating calcite substrates, often at the tips of thin, elongated calcite blades (Paces et al., 1998a). Micrometer-scale layering is optically detected under high magnification in even the thinnest opal sheets and smallest hemispheres (Fig. 2 in Neymark and Paces, 2000).

Twenty-six opal samples analyzed for U–Th–Pb isotopes represent outermost layers of 16 secondary mineral coatings collected in the Exploratory Studies Facility (ESF). The ESF is a tunnel, 8 km long and 7.6 m in diameter, excavated beneath Yucca Mountain to the level of the potential repository horizon. Samples were collected between ESF distances 2272 and 7990 m from the north portal of the tunnel at depths of about 10–290 m below the land surface. The selection was based on previously obtained U-series opal data from outermost surfaces of fracture- and cavity-coating deposits (Paces et al., 1998a, 2000) that contained high U abundances (>50 ppm), had $^{230}\text{Th}/\text{U}$ ages between 50 and 300 ka, and initial $^{234}\text{U}/^{238}\text{U}$ activity ratios between 2 and 10.

3. METHODS

3.1. Analytical Techniques

Opal fractions were separated at the U.S. Geological Survey (USGS) laboratory in Denver, Colorado, under the binocular microscope by prying with a sharp needle thin opal sheets or hemispheres from outermost growth surfaces that sometimes contained admixed or intergrown calcite. Bright fluorescence of opal under short-waved UV illumination was used to improve separation of the two phases. The thinnest opal sheets analyzed are on the order of tenths of a millimeter thick (typically 0.1–0.3 mm), which is still up to two orders of magnitude greater than the finest laminations and smallest micrometer-scale spheres observed in the opals by scanning electron microscopy (unpublished data of the authors). The work was done in two stages. In the first stage, aliquots of the same samples were analyzed for $^{230}\text{Th}/^{234}\text{U}/^{238}\text{U}$ at the Denver laboratory, and for U–Pb and $^{234}\text{U}/^{238}\text{U}$ at the Jack Satterly Geochronology laboratory, Royal Ontario Museum (ROM), Toronto, Canada. In the second stage, all the analyses were done in the Toronto laboratory using a Pb–Th–U mixed spike solution.

The U-series analytical technique for the USGS laboratory has been described in detail elsewhere (Neymark and Paces, 2000). Total procedural blanks were about 5 pg ^{238}U , 0.0003–0.001 pg ^{234}U , 20 pg ^{232}Th , and <0.0004–0.001 pg ^{230}Th . Multiple analyses of a solution of secular equilibrium material (\approx 70-Ma-old uranium ore; Ludwig et al., 1985) gave calculated $^{234}\text{U}/^{238}\text{U}$ and $^{230}\text{Th}/^{238}\text{U}$ activity ratios that were within analytical error of unity.

In the ROM laboratory the opal (plus calcite, if present) chips were broken in an alumina mortar under ethanol, and the ethanol decanted several times to remove fine particles. Opal fragments of uniform appearance were hand-picked under a binocular microscope and examined for visible imperfections against white and black backgrounds at high magnification. The opal fractions were then washed in ultrapure water with ultrasonic agitation to remove surface contamination, and subsequently leached mildly with high purity 2 N HCl at room temperature. Experiments discussed below show that this acid treatment does not appreciably disturb the U–Th–Pb system in the opal residues. These methods provided samples of pure opal without adhering calcite, ranging in weight from 0.033 to 3.5 mg. Finally, the samples were rinsed several times with ultra-pure water and distilled acetone, dried in a clean air flow, spiked with a $^{235}\text{U}/^{205}\text{Pb}$ mixed tracer solution, and digested in HF + HNO₃ in Teflon vials at 100°C. Pb and U were separated chemically using anion exchange resins in Teflon microcolumns (Krogh, 1973). The purified Pb and U fractions were loaded on Re filaments with a H₃PO₄–silica gel mixture and run as Pb⁺ and UO₂⁺ ions in a VG 354 thermal-ionization mass spectrometer. Total procedure blanks during this stage of the study were 1.5 ± 1.0 and 0.1 ± 0.05 pg for Pb and U, respectively.

In the second stage of the study a Pb–Th–U mixed spike tracer solution was used to avoid potential problems with sample age heterogeneity, possibly causing discordant U–Pb and U-series data obtained for sample aliquots during the first stage of this study (as discussed later). The calibration of the ^{205}Pb – ^{229}Th – ^{233}U – ^{236}U tracer solution was checked by spiking three different geologically old, standard samples (a uranium ore and two zircons). The U–Pb systems of these standard materials were proven to be closed (Ludwig et al., 1985;

Table 1. U–Th–Pb concentrations and isotope data for secular equilibrium standard materials.

| Wt. (mg) | U (ppm) | ²³² Th (ppm) | Pb (ppm) | ²⁰⁶ Pb/ ²⁰⁴ Pb ^a | ²⁰⁶ Pb*/ ²³⁸ U ^a | ²⁰⁷ Pb*/ ²³⁵ U | Rho ^b 6/8–7/5 | ²³⁰ Th/ ²³⁸ U Activity | ²³⁴ U/ ²³⁸ U Activity |
|--|---------|-------------------------|----------|---|---|--------------------------------------|--------------------------|--|---|
| SU-1 (solution of ~69 Ma Schwartzwalder uranium ore) | | | | | | | | | |
| 35.25 | 12.43 | 0.00888 | 1.406 | 38.124 (0.14) ^c | 0.0253 (4.6) | 0.267 (6.6) | 0.799 | 1.003 (0.62) | 0.999 (0.43) |
| 32.78 | 11.86 | 0.01518 | 1.334 | 38.141 (0.10) | 0.0252 (4.3) | 0.268 (6.2) | 0.792 | 0.995 (1.3) | 0.997 (0.35) |
| 32.65 | 12.29 | 0.01424 | 1.382 | 38.136 (0.09) | 0.0252 (4.2) | 0.267 (6.2) | 0.792 | 0.998 (1.1) | 0.997 (0.30) |
| 26.67 | 12.31 | 0.00788 | 1.390 | 38.127 (0.10) | 0.0253 (4.2) | 0.268 (6.2) | 0.791 | 0.998 (1.1) | 0.998 (0.41) |
| 91500 (~1065 Ma zircon, Ontario, Canada) | | | | | | | | | |
| 0.045 | 78.19 | ND ^d | ND | ND | ND | ND | | ND | 0.997 (0.64) |
| 0.031 | 76.22 | ND | 13.87 | 85,759 | 0.1789 (0.30) | 1.846 (0.31) | 0.962 | ND | 0.998 (0.86) |
| 0.042 | 73.11 | ND | 13.33 | 77,675 | 0.1791 (0.34) | 1.850 (0.40) | 0.855 | ND | 1.000 (1.4) |
| 0.012 | 82.51 | ND | 14.99 | 27,494 | 0.1782 (0.35) | 1.838 (0.37) | 0.957 | ND | 0.995 (5.0) |
| 61308B (~2.5 Ma zircon, France) | | | | | | | | | |
| 0.151 | 225.9 | 391.1 | ND | ND | ND | ND | ND | 1.06 (9.1) | 0.997 (0.42) |
| 0.247 | 187.4 | 269.3 | ND | ND | ND | ND | ND | 0.974 (2.6) | 1.003 (0.28) |
| 0.252 | 182.3 | 287.7 | ND | ND | ND | ND | ND | 0.989 (3.1) | 1.002 (0.48) |
| 0.238 | 172.0 | 241.0 | ND | ND | ND | ND | ND | 0.98 (13) | 1.001 (0.23) |

^a Ratios corrected for procedural blank, mass discrimination, and common lead.

^b Error correlation between ²⁰⁷Pb*/²³⁵U and ²⁰⁶Pb*/²³⁸U.

^c Numbers in parentheses are 2σ errors in percent.

^d ND, not determined.

Wiedenbeck et al., 1995) and are assumed to be in secular radioactive equilibrium with regard to uranium and its decay products. Concentrations and isotopic data for these standards are given in Table 1 and Figure 1. Average measured ²³⁴U/²³⁸U and ²³⁰Th/²³⁸U activity ratios are equal to unity within the error limits and U–Pb data are nearly concordant (Fig. 1).

Cleaned opal fractions were spiked with the mixed ²⁰⁵Pb–²²⁹Th–²³³U–²³⁶U tracer solution and digested in HF + HNO₃ in Teflon vials at 100°C. Because opal samples analyzed in this study are essentially iron free, Pb and U were separated using anion-exchange resin in HCl media, similar to the chemical procedure used by Amelin et al. (1994) for small zircon fractions. This procedure uses a minimum amount of reagents resulting in a low Pb blank that is crucial for this study. Eluates of the anion-exchange columns, containing the bulk cation load including Th, were reprocessed through the same columns in 7 N HNO₃ and 6 N HCl (Tatsumoto, 1966) to separate pure Th fractions. Samples were loaded on outgassed Re filaments with silica gel for Pb analyses or between layers of colloidal graphite for U and Th analyses following Edwards et al. (1987). All three elements were analyzed with a VG-354 mass spectrometer using a single Daly photomultiplier in analog mode. Average total blanks for this procedure were 1.0 pg Pb, 1.6 pg ²³⁸U, 4.7 pg ²³²Th, and 0.005 pg ²³⁰Th, with ≈50% relative 2σ errors. Total procedural blanks for Th and U were dominated by emission from graphite-coated Re filaments (for comparison, the mean ²³⁸U total procedural blank at ROM was 0.1 ± 0.05 pg when measured as UO₂⁺ from SiO₂ loads). In spite of the advantage in lower U blanks of SiO₂ loads, the graphite technique was used at the second stage of this work, because of the higher ionization efficiency allowing better counting statistics for ²³⁴U from small submilligram-sized opal samples.

The resulting Pb and U isotopic data were reduced using the PBDAT program (Ludwig, 1988) correcting for mass fractionation, procedural blank, spike contribution, and initial common Pb. The isotopic composition of the Pb blank was determined as 17.95 ± 1.53 for ²⁰⁶Pb/²⁰⁴Pb, 15.31 ± 1.05 for ²⁰⁷Pb/²⁰⁴Pb, and 36.68 ± 2.79 for ²⁰⁸Pb/²⁰⁴Pb (median values of all blank measurements during the course of this study), with an error correlation coefficient of 0.8 between ²⁰⁷Pb/²⁰⁴Pb and ²⁰⁶Pb/²⁰⁴Pb. The common-lead correction is particularly critical for young samples with low concentrations of radiogenic Pb. Because no correlation between measured ²⁰⁶Pb/²⁰⁴Pb and sample sizes was observed, all common Pb remaining after blank subtraction was assumed to have natural origin. The common Pb correction was done using mean values of Pb isotope compositions for seven samples of filtered groundwater from Yucca Mountain and 22 samples of subsurface Quaternary calcite with low U/Pb ratios (Zartman and Kwak, 1993, and 1995, written communication) of 15.62 ± 0.09 (²⁰⁷Pb/²⁰⁴Pb), 18.83 ± 0.82

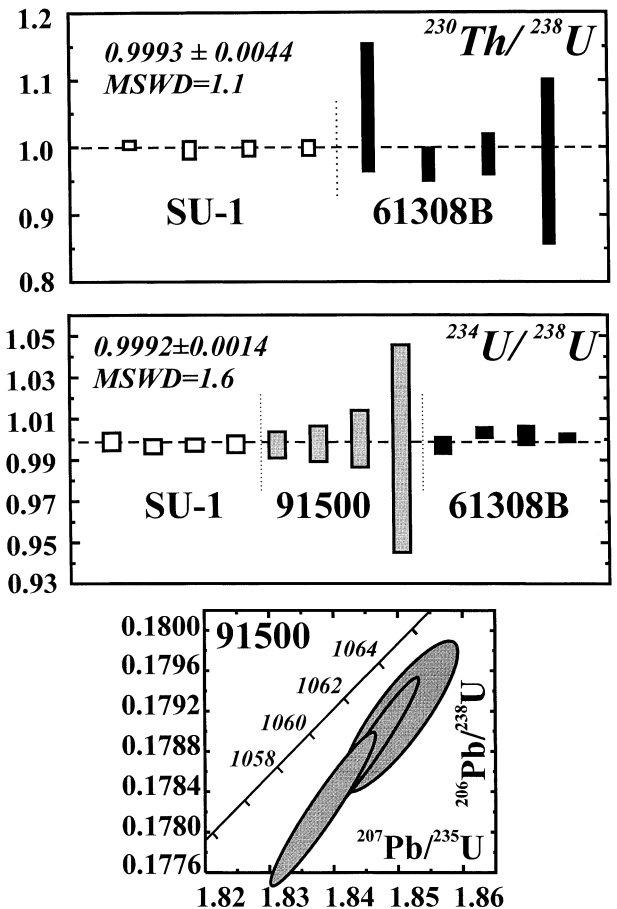


Fig. 1. U–Th–Pb isotope results for different standard materials obtained using a ²²⁹Th–²³³U–²³⁶U–²⁰⁵Pb mixed spike. Analytic data are from Table 1. Measured ²³⁰Th/²³⁸U and ²³⁴U/²³⁸U activity ratios are unity within the error limits. U–Pb data show a small degree of discordance, consistent with the results reported by Wiedenbeck et al. (1995).

($^{206}\text{Pb}/^{204}\text{Pb}$), and 38.78 ± 0.53 ($^{208}\text{Pb}/^{204}\text{Pb}$). Disequilibrium U–Pb and U-series ages and $^{234}\text{U}/^{238}\text{U}$ initial activity ratios were calculated using the ISOPLOT program (Ludwig, 1997). The presence of measurable ^{232}Th was assumed to indicate a nonhydrogenic (particulate) contaminant in the subsample that contributes atoms of ^{230}Th not related to in situ uranium decay. Opal $^{234}\text{U}/^{238}\text{U}$ and $^{230}\text{Th}/^{238}\text{U}$ compositions are determined by subtracting from measured ratios a secular equilibrium detrital component with an atomic Th/U ratio of 6 ± 3 (average of unaltered and altered Yucca Mountain tuffs; Neymark et al., 1995) using the measured $^{232}\text{Th}/^{238}\text{U}$ to define the amount of the contaminant. Corrected $^{234}\text{U}/^{238}\text{U}$ and $^{230}\text{Th}/^{238}\text{U}$ ratios are used to calculate $^{230}\text{Th}/^{238}\text{U}$ ages and initial $^{234}\text{U}/^{238}\text{U}$ ratios using the conventional equation relating ^{230}Th to ^{238}U as a function of time (Kaufman and Broecker, 1965) as formulated in the program ISOPLOT (Ludwig, 1997). All reported errors correspond to a 95% confidence level. Decay constants used in the calculations are: $\lambda^{238}\text{U} = 1.55125 \times 10^{-10}\text{y}$, $\lambda^{235}\text{U} = 9.8485 \times 10^{-10}\text{y}$, $\lambda^{234}\text{U} = 2.835 \times 10^{-6}\text{y}$, $\lambda^{230}\text{Th} = 9.1952 \times 10^{-6}\text{y}$, $\lambda^{226}\text{Ra} = 4.332 \times 10^{-4}\text{y}$, $\lambda^{210}\text{Pb} = 3.151 \times 10^{-2}\text{y}$, $\lambda^{231}\text{Pa} = 2.133 \times 10^{-5}\text{y}$, $\lambda^{227}\text{Ac} = 3.151 \times 10^{-2}\text{y}$ (De Bièvre et al., 1971; Jaffey et al., 1971; Lounsbury and Dunham, 1971; Meadows et al., 1980; Browne and Firestone, 1986).

3.2. Principles of combined $^{206}\text{Pb}/^{230}\text{Th}/^{234}\text{U}/^{238}\text{U}$ and $^{207}\text{Pb}/^{235}\text{U}$ dating

The conventional method (Faure, 1986) of calculating U–Pb isotope ages from observed common lead-corrected $^{207}\text{Pb}^*/^{235}\text{U}$ and $^{206}\text{Pb}^*/^{238}\text{U}$ ratios (see Appendix 1, Eqns. A1 and A2) assumes that all intermediate daughter isotopes were in secular equilibrium at the time of mineral formation (activity of all daughter isotopes was equal to that of the parent). This assumption is not truly valid for most natural systems because of differences in geochemical behavior of parent and daughter elements (e.g., U, Th, Pa, Ac, and Ra). Nevertheless, the conventional radioactive decay equations (Eqns. A1 and A2) still give accurate U–Pb age estimates for geologically old (>100 Ma) samples in cases of moderate elemental fractionation during formation of a mineral geochronometer because the effects of the initial radioactive disequilibrium are smaller than analytic uncertainties of measuring Pb/U ratios. In systems older than 1.5 Ma, for example, there is an absolute difference of about 0.0005 between $^{206}\text{Pb}^*/^{238}\text{U}$ ratios calculated for $^{234}\text{U}/^{238}\text{U}$ initial activity ratios of 1 and 10. This difference is about 50% of the ratio's value for 2-Ma-old samples but only 3% for 100 Ma and 0.24% for 1 Ga samples.

In the case of Yucca Mountain opals of Quaternary age where extreme U–Th–Pb elemental fractionation and ^{234}U enrichment are observed (see following sections) it becomes necessary to use decay equations that take into account initial radioactive disequilibria of the uranium daughters. The more general forms of age equations for a closed system are used for this study (see Appendix 1, Eqns. A3 through A7; Bateman, 1910; Catchen, 1984). These equations consider only the daughter isotopes with half-lives more than 1 yr and are applicable to systems older than 1000 yr. They take into account initial disequilibrium of $^{234}\text{U}/^{238}\text{U}$, and assume negligible initial ^{231}Pa , ^{227}Ac , ^{230}Th , ^{226}Ra , ^{210}Pb , ^{207}Pb , and ^{206}Pb (Ludwig, 1977; Wendt and Carl, 1985).

The initial absence of Th, Ac, Pa, and Pb isotopes from uranium decay chains in minerals precipitated from oxidizing aqueous solutions is a reasonable assumption because of low solubilities and short residence times of these elements relative to uranium in groundwater (Gascoyne, 1992). Uranium can be readily dissolved during weathering, alteration, or water/rock interaction and can be transported as a carbonate, sulfate, phosphate, or silicate complex as long as Eh is sufficiently high to keep U in a hexavalent state (Langmuir, 1978). In contrast, thorium is present only in a tetravalent form, and, as such, is insoluble in oxidizing waters of near neutral pH (Langmuir and Herman, 1980). Colloidal transport of Th (Osthols, 1995) is also unlikely for the range of pH from 6.5 to 9.4, which is typical for water at Yucca Mountain (Meijer, 1990). Unlike Th and the other insoluble elements, radium is present in the natural environment as Ra^{2+} species and chemically behaves similarly to barium (i.e., is water soluble). Excesses of ^{226}Ra over its parent ^{230}Th have been reported in soils (Dickson and Wheller, 1992; Olley et al., 1997). Given the low hydrochemical mobility of Th, the presence of these excesses indicates that

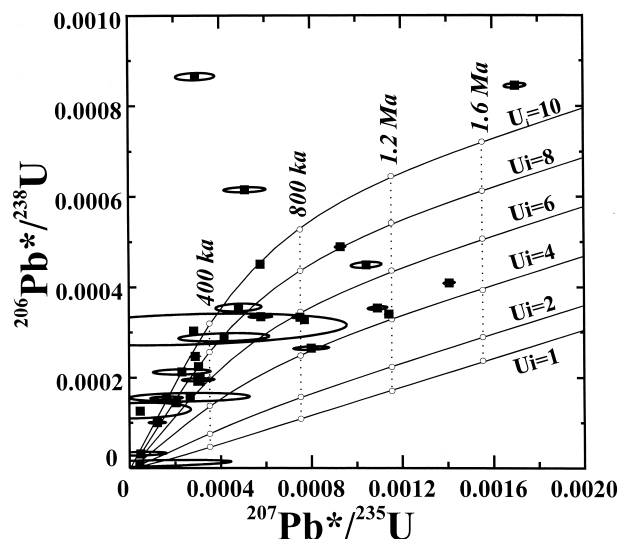


Fig. 2. A concordia diagram for the case of initial radioactive disequilibrium. Common lead-corrected $^{206}\text{Pb}^*/^{238}\text{U}$ and $^{207}\text{Pb}^*/^{235}\text{U}$ ratios for Yucca Mountain opals are plotted together with a series of concordia curves corresponding to $^{234}\text{U}/^{238}\text{U}$ initial activity ratios (U_i) of 1, 2, 4, 6, 8, and 10. U–Pb isotope data are shown as 2σ error ellipses. The error correlation is almost zero for points with high common lead correction causing high uncertainties in $^{207}\text{Pb}^*/^{235}\text{U}$ ratios. The distribution of the data indicates variations of $^{234}\text{U}/^{238}\text{U}$ initial activity ratios between values 2 and >10. Isochrons are shown as vertical dotted lines connecting points of equal age on the concordia curves.

radium is mobile in the soil zone and potentially can be transported by meteoric water as it percolates downward.

Measured present-day values of $^{206}\text{Pb}^*/^{238}\text{U}$ and $^{207}\text{Pb}^*/^{235}\text{U}$ yield two independent apparent ages for the same material based on the two different radioactive parent isotopes (Faure, 1986). Concordance of ages between these two systems is an important check on the closed system behavior of the material analyzed with regard to gains or losses of uranium and its daughter nuclides. However, in the case of initial ^{234}U enrichment for geologically young materials, even for an undisturbed mineral the equilibrium $^{206}\text{Pb}^*/^{238}\text{U}$ age will be older than the $^{207}\text{Pb}^*/^{235}\text{U}$ age because of additional amounts of $^{206}\text{Pb}^*$ derived from the initial excess of ^{234}U . In such a situation the calculation of the correct $^{206}\text{Pb}^*/^{238}\text{U}$ age requires a knowledge of the initial $^{234}\text{U}/^{238}\text{U}$ activity ratio (see Eqn. A6). Previous U-series data indicated that initial $^{234}\text{U}/^{238}\text{U}$ activity ratios for Yucca Mountain subsurface opal are elevated ranging from 2 to 10 (Paces et al., 1998a; Neymark and Paces, 2000). Therefore, it is difficult to make any plausible a priori assumption constraining the value of this ratio and a family of concordia curves for different $^{234}\text{U}/^{238}\text{U}$ initial activity ratios is needed to describe the U–Pb systems (Fig. 2; data points shown in Figs. 2 through 5 will be discussed in following sections of the paper). The shape of the concordia curves reflects fast growth of radiogenic $^{206}\text{Pb}^*$ derived from the excess ^{234}U during the first 1 Ma of a mineral life, after which ^{234}U reaches radioactive equilibrium with ^{238}U and the curves become parallel to each other. The $^{207}\text{Pb}^*/^{235}\text{U}$ age is independent from the unknown initial $^{234}\text{U}/^{238}\text{U}$ unlike the apparent age based on $^{206}\text{Pb}^*/^{238}\text{U}$. Consequently, isochrons (loci of data points for coeval samples) in this plot are represented by a series of vertical lines (Fig. 2).

A standard $^{230}\text{Th}/\text{U}$ dating technique can be applied to young (<500 ka) samples for both the age and uranium initial activity ratio determination using a $^{230}\text{Th}/^{238}\text{U}$ – $^{234}\text{U}/^{238}\text{U}$ evolution diagram (Fig. 3). Isochrons in this diagram are fan-like, because values for both axes depend on initial $^{234}\text{U}/^{238}\text{U}$. This technique is applicable only to materials younger than ≈ 500 ka even for the most precise mass spectrometric data (Edwards et al., 1987) because it is limited by the relatively short (≈ 75 kyr) half-life of ^{230}Th . Another disadvantage of

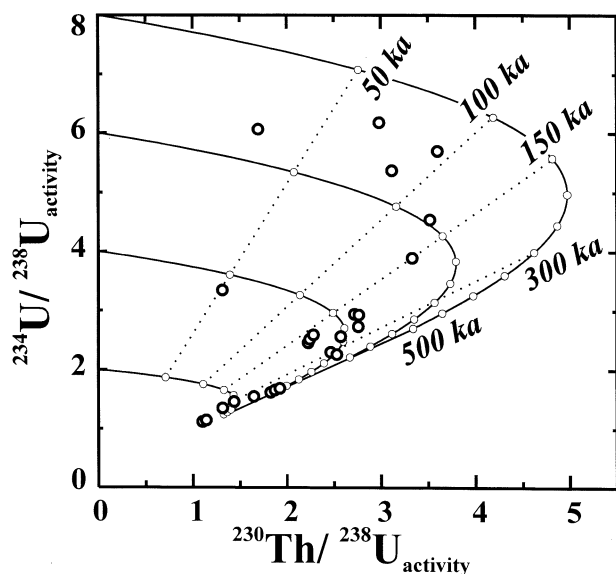


Fig. 3. $^{234}\text{U}/^{238}\text{U}$ vs. $^{230}\text{Th}/^{238}\text{U}$ evolution diagram for Yucca Mountain opals. Errors are smaller than symbol sizes. Curved lines (evolution curves) represent loci of $^{230}\text{Th}/^{238}\text{U}$ and $^{234}\text{U}/^{238}\text{U}$ activity ratios that will develop through time in a material with initial $^{234}\text{U}/^{238}\text{U}$ activity ratios (U_i) of 2, 4, 6, and 8. Ticks on the evolution curves are for ages in 50 ka intervals. Fan-like isochrons are also shown.

this dating technique is the lack of internal check for closed system behavior.

An independent U-series age also can be calculated from the $^{234}\text{U}/^{238}\text{U}$ ratio alone for materials with today's $^{234}\text{U}/^{238}\text{U}$ activity ratios greater than unity, extending the datable interval to ≈ 1.5 Ma, because of the slower decay of ^{234}U (half-life of ≈ 245 kyr) than that of ^{230}Th . The age can be calculated using the measured $^{234}\text{U}/^{238}\text{U}$ ratio from Eqn. A8, only if the $^{234}\text{U}/^{238}\text{U}$ initial activity ratio is known. A new approach was developed to resolve this problem by combining the measured $^{234}\text{U}/^{238}\text{U}$ with any other time-dependent isotope ratio from the U-series decay chain, for example, $^{206}\text{Pb}^*/^{238}\text{U}$ or $^{207}\text{Pb}^*/^{235}\text{U}$, to obtain the age and $^{234}\text{U}/^{238}\text{U}$ initial activity ratio. The two new concordia plots (Fig. 4a,b) show a series of concordia curves corresponding to different $^{234}\text{U}/^{238}\text{U}$ initial activity ratios. These curves are divergent for younger ages, but get closer to each other for older ages and almost coincide for ages older than ≈ 1.5 Ma, thus reflecting radioactive decay of an initially present excess of ^{234}U . The difference between the two plots is that isochrons are fan-like in Figure 4a and vertical in Figure 4b. The latter diagram involves ^{234}U , but not ^{206}Pb , and thus can be used as an indicator of possible irregularities at the succeeding ^{234}U late stages of the ^{238}U decay chain. Discrepancies between the ages obtained from this diagram, and those obtained from previously discussed plots, may indicate initial presence of ^{230}Th or ^{226}Ra , or ^{222}Rn leakage.

A link between measured $^{230}\text{Th}/^{238}\text{U}_{\text{activity}}$ and $^{206}\text{Pb}^*/^{238}\text{U}$ ratios, both of which are time dependent, allows another concordia plot (Fig. 5). The concordia curves in this plot are bell-shaped because of the combination of in-growth and decay of initially absent ^{230}Th . An analogous $^{207}\text{Pb}^*/^{235}\text{U}$ vs. $^{230}\text{Th}/^{238}\text{U}_{\text{activity}}$ diagram (not shown) can also be created. The isochrons are fan-like in Figure 5 and vertical in the $^{207}\text{Pb}^*/^{235}\text{U}$ vs. $^{230}\text{Th}/^{238}\text{U}_{\text{activity}}$ diagram. All six plots discussed above represent projections of a single four-dimensional concordia diagram with $^{230}\text{Th}/^{238}\text{U}_{\text{activity}}$, $^{234}\text{U}/^{238}\text{U}_{\text{activity}}$, $^{206}\text{Pb}^*/^{238}\text{U}$, and $^{207}\text{Pb}^*/^{235}\text{U}$ axes.

4. RESULTS

4.1. Leaching Experiments

The laboratory acid treatment used to eliminate surface contamination of the opal samples and to separate opal from

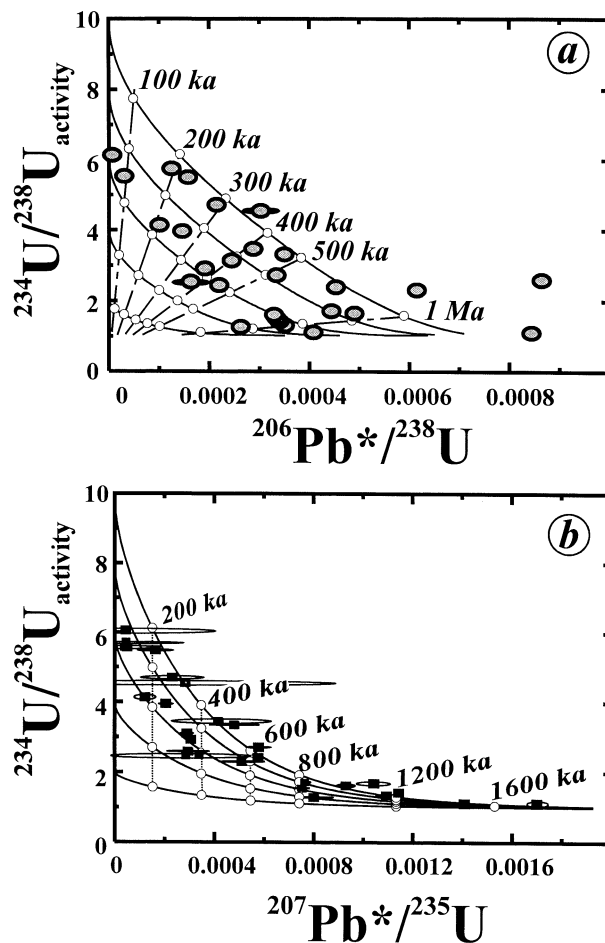


Fig. 4. New $^{234}\text{U}/^{238}\text{U}$ – $^{206}\text{Pb}^*/^{238}\text{U}$ (a) and $^{234}\text{U}/^{238}\text{U}$ – $^{207}\text{Pb}^*/^{235}\text{U}$ (b) concordia diagrams showing data for Yucca Mountain opals. U–Pb isotope data are shown as 2σ error ellipses if larger than symbol size. A family of evolution curves corresponding to $^{234}\text{U}/^{238}\text{U}$ initial activity ratios of 2, 4, 6, 8, and 10 and isochrons connecting points of equal age on these curves are also shown.

adherent calcite was evaluated in two series of experiments to estimate the potential effects on the U–Th–Pb systems.

The first leaching series evaluated acetic acid vs. HCl and different HCl concentrations and exposures on U–Th fractionation. A large (several hundred milligrams) fracture coating sample representing an approximately 10:1 mixture of calcite and opal was powdered for homogenization, then split into five powder aliquots, and subjected to acid leaching with varying acid concentrations and exposure times. The results showed a lack of ^{230}Th fractionation relative to U in opal residues (Neymark and Paces, 2000).

The second series of experiments was performed during this study and evaluated how leaching may affect pure opal in sample HD2179Pb2, which did not contain any visible admixtures of calcite. Sixteen fragments of very clear, hard opal with a concentric ring surface texture were hand-picked and washed with ultrasonic agitation in distilled H_2O . Four fragments (total weight, 0.151 mg) then were spiked with a U–Th–Pb isotope tracer and subjected to dissolution without further acid leaching. These four fragments, called HD2179Pb2-2, represented

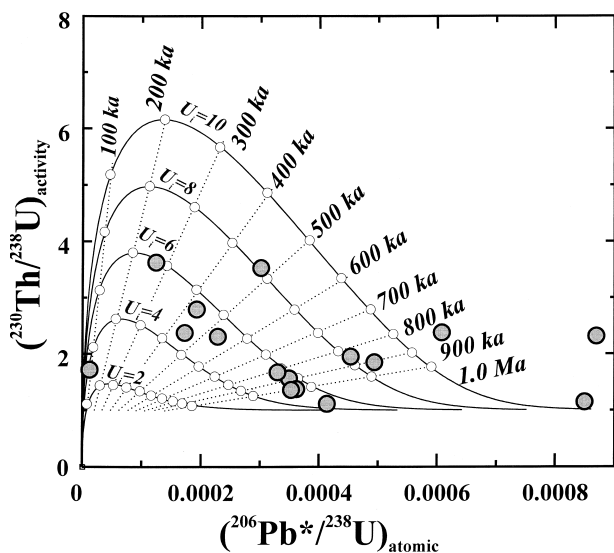


Fig. 5. A new $^{230}\text{Th}/^{238}\text{U}$ vs. $^{206}\text{Pb}^*/^{238}\text{U}$ concordia diagram for Yucca Mountain opals. Symbol sizes are larger than 2σ errors. Bell-shaped concordia curves for U_i of 2, 4, 6, 8, and 10 and a family of fan-like isochrons is also shown.

unleached opal. The remaining 12 fragments (total weight, 0.805 mg) were leached in 0.2 mL of 2 N HCl at 20°C for 30 min including ultrasonic agitation for 1 min. The leachate (L1) was removed by pipette and the residue was rinsed with distilled acetone and weighed. Sample loss at this first leaching stage was 0.002 mg. Then the residue was leached again with 0.2 mL of 2 N HCl at 100°C for 3 h and the leachate (L2) was separated. The weight loss at the second leaching stage was also 0.002 mg. The sequential leachates (L1 and L2) and the residue (HD2179Pb2-3) were spiked with a ^{233}U – ^{236}U – ^{229}Th – ^{205}Pb mixed isotope tracer and analyzed for U, Th, and Pb concentrations and isotopic compositions. The results are presented in Table 2, and data for the total digest (HD2179Pb2-2) and residue (HD2179Pb2-3) are also given in Tables 3 and 4. Concentrations of U and Pb are close in the unleached sample and recombination of leachate–residue data (Table 2). The sample heterogeneity or different degrees of surface contamination may cause some discrepancies between the results (in Th concentration, in particular).

Several important observations can be made on the basis of this series of leaching experiments:

1. The data demonstrate that fragments of hard and clear opal hemispheres cannot be appreciably dissolved even in a hot 2 N HCl solution, because the total weight loss after two sequential leachates did not exceed 0.5% of the initial sample weight.
2. HCl leaching removed only minute amounts of U; the residue after leaching contained 99.98% of the total uranium (Table 2).
3. Acid leaching effectively removed Th ($\approx 85\%$) and Pb ($\approx 24\%$) from the opal, which are predominantly ^{232}Th and common lead (Table 2), most reasonably derived from surface contamination during sample treatment.
4. No difference was observed in the $^{230}\text{Th}/^{238}\text{U}$ ratio between the unleached sample and the residue (Table 2).

Summarizing the results of the leaching experiments, the laboratory acid treatment, which is necessary to separate opal from adherent calcite and to eliminate surface contamination, did not appreciably affect U–Th–Pb isotopic systems in opals. The experiments also showed that opal has a considerable resistance to short-lived interactions with reactive media with regard to loss of uranium and its daughter decay products.

4.2. U, Th, and Pb Concentrations and Isotopic Compositions

Concentrations of U, Th, and Pb, in the subsurface opals vary from 30 to 313 ppm, 0.75 to 3740 ppb, and 8.9 to 83.3 ppb, respectively, resulting in a range of Th/U ratios from 0.013 to values as low as 7.5×10^{-6} (Table 3). Extremely low Th abundance may be caused by poor solubility of Th in groundwater as well as by elimination of particulate-related Th by filtration of water percolating downward through the overlying rock mass. Very low common lead content, along with elevated uranium, results in extremely high $^{238}\text{U}/^{204}\text{Pb}$ measured in the opals ($n \times 10^5$ to $n \times 10^8$; Table 3), which is comparable to the typical $^{238}\text{U}/^{204}\text{Pb}$ ratio in zircon—one of the best U–Pb mineral geochronometers. The lead isotopic compositions have elevated radiogenic ^{206}Pb and ^{207}Pb , and low ^{208}Pb and measured $^{206}\text{Pb}/^{204}\text{Pb}$ ratios vary from 24.0 to 11,370, most analyses having blank-corrected $^{206}\text{Pb}/^{204}\text{Pb}$ ratios greater than 100 (Table 3). In small samples, most of the ^{204}Pb is due to the blank causing errors often exceeding 100% in blank-corrected $^{206}\text{Pb}/^{204}\text{Pb}$, $^{206}\text{Pb}/^{207}\text{Pb}$, and $^{206}\text{Pb}/^{208}\text{Pb}$ ratios; however, the errors reported for blank- and common lead-corrected $^{206}\text{Pb}^*/^{238}\text{U}$ (0.33–13%) and $^{207}\text{Pb}^*/^{235}\text{U}$ (typically 2–40%) remain much smaller because of error correlation effects. The highest errors in $^{207}\text{Pb}^*/^{235}\text{U}$ (200–740%) were obtained for four samples with either an elevated common Pb content (HD2065Pb2 and HD2055Pb4), or a very young, less than 100 ka, mineral age (HD2098).

All opal samples contain excess ^{234}U and ^{230}Th relative to ^{238}U . Measured $^{234}\text{U}/^{238}\text{U}$ and $^{230}\text{Th}/^{238}\text{U}$ activity ratios vary from 1.117 to 6.179 and from 1.102 to 3.600, respectively (Table 3). Extremely low $^{232}\text{Th}/^{230}\text{Th}$ activity ratios (typically 10^{-6} to 10^{-3} ; Table 3) in most cases rendered a correction for the potential presence of initial terrigenous ^{230}Th for $^{230}\text{Th}/\text{U}$ age calculations inconsequential relative to analytical uncertainties.

4.3. Apparent Ages and Initial $^{234}\text{U}/^{238}\text{U}$ Activity Ratios

Calculated equilibrium $^{206}\text{Pb}^*/^{238}\text{U}$ and $^{207}\text{Pb}^*/^{235}\text{U}$ ages for Yucca Mountain opals display strong reverse discordance, that is, data points plot above the concordia curve derived assuming an initial $^{234}\text{U}/^{238}\text{U}_{\text{activity}} = 1$ (Table 3, Fig. 2). Most of the data points plot within the coordinates predicted by closed system decay of U having initial disequilibrium in the range typically observed for surface and subsurface materials at Yucca Mountain ($^{234}\text{U}/^{238}\text{U}$ activity ratios 2–10; Paces et al., 1998a, 2000; Neymark and Paces, 2000). Radiogenic $^{207}\text{Pb}^*/^{206}\text{Pb}^*$ ratios range between 0.0025 and 0.0347, and all are below the present-day equilibrium value of 0.0461, thus resulting in negative apparent ages. In some cases these ages are incalculable because observed $^{207}\text{Pb}^*/^{206}\text{Pb}^*$ is lower than the

Table 2. U, Th, and Pb concentrations and isotopic compositions for leaching experiments with sample HD2179Pb2.

| Sample name and leaching conditions | Weight (mg) | Fraction of | | Fraction of | | Fraction of | | Pb (ppb) | Fraction of | | | | |
|-------------------------------------|--------------|------------------|------------------------|-------------|-------------------------|--------------|---|-------------|--|---------------|---|---|---|
| | | total weight (%) | ²³⁸ U (ppm) | total U (%) | ²³² Th (ppm) | total Th (%) | ²³⁴ U/ ²³⁸ U ^b | | ²³⁰ Th/ ²³⁸ U ^b | total Pb (%) | ²⁰⁶ Pb/ ²⁰⁴ Pb ^c | ²⁰⁷ Pb/ ²⁰⁴ Pb ^c | ²⁰⁸ Pb/ ²⁰⁴ Pb ^c |
| HD2179-Pb2-2 | | | | | | | | | | | | | |
| Total digestion | 0.151 | 100 | 54.98 | 100 | 0.332 | 100 | 2.645 (0.8) | 2.265 (2.2) | 17.16 | 100 | 81.44 | 16.39 | 38.77 |
| HD2179-Pb2-3 | | | | | | | | | | | | | |
| L1, 30 min, 2N HCl, 20°C | 0.002 | 0.25 | 2.47 | 0.01 | 4.108 | 52.82 | ND | ND | 795 | 11.08 | 18.96 | 15.74 | 36.08 |
| L2, 3 h, 2N HCl, 100°C | 0.002 | 0.25 | 1.70 | 0.01 | 2.468 | 31.73 | ND | ND | 909 | 12.67 | 18.21 | 15.62 | 37.57 |
| L1 + L2 ^a | <i>0.004</i> | <i>0.50</i> | <i>2.08</i> | <i>0.02</i> | <i>3.288</i> | <i>84.55</i> | <i>ND</i> | <i>ND</i> | <i>852</i> | <i>23.75</i> | <i>18.56</i> | <i>15.68</i> | <i>36.87</i> |
| Residue | 0.801 | 99.50 | 56.08 | 99.98 | 0.003 | 15.45 | 2.518 (0.4) | 2.249 (0.8) | 13.66 | 76.25 | 289.8 | 18.49 | 41.96 |
| L + R ^a | <i>0.805</i> | <i>100</i> | <i>55.81</i> | <i>100</i> | <i>0.019</i> | <i>100</i> | <i>ND</i> | <i>ND</i> | <i>17.83</i> | <i>100.00</i> | <i>126.3</i> | <i>16.79</i> | <i>38.89</i> |

^a Mathematically recombined values are given in italics.

^b Measured activity ratios with relative 2σ errors (in %) given in parentheses.

^c Spike, blank, and mass discrimination corrected ratios.

ND, not determined.

lowest theoretic limit for this ratio of 0.00725, which will be reached with radioactive equilibrium in approximately 50 billion yr when all terrestrial ²³⁸U has decayed. Equilibrium ²⁰⁶Pb*/²³⁸U ages range from 60 ka to 5.57 Ma, whereas the ²⁰⁷Pb*/²³⁵U equilibrium ages are systematically younger and define a smaller range of 50 ka to 1.73 Ma. Correlation between errors of ²⁰⁷Pb*/²³⁵U and ²⁰⁶Pb*/²³⁸U is low (highest correlation coefficient Rho = 0.51; Table 3) because very small amounts of radiogenic ²⁰⁷Pb are much more sensitive to increases in common lead. Disequilibrium ²⁰⁷Pb*/²³⁵U ages, calculated assuming zero initial abundance of ²³¹Pa and ²²⁷Ac, are ≈50 ka older than the corresponding equilibrium ²⁰⁷Pb*/²³⁵U ages (Table 4). An application of two new concordia diagrams ²⁰⁶Pb*/²³⁸U–²³⁴U/²³⁸U and ²⁰⁶Pb*/²³⁸U–²³⁰Th/²³⁸U (Figs. 4a and 5) gives apparent ages ranging from 50 ± 9 to 1595 ± 285 ka and 39 ± 14 to 1021 ± 30 ka, respectively (Table 4). These age estimates are much more precise than ²⁰⁷Pb*/²³⁵U ages.

No ²³⁰Th unsupported by ²³⁴U was detected, and in all cases it was possible to calculate finite ²³⁰Th/U ages in the range from 34.1 ± 0.6 to ≈465 ka (Fig. 3, Table 4). These ages are within the range previously observed for Yucca Mountain fracture- and cavity-coating calcite and opal (Neymark and Paces, 1996, 2000; Paces et al., 1996, 1998a).

The isotopic data allow different ways for calculating initial ²³⁴U/²³⁸U activity ratios (U_i) in the analyzed opals using plots shown in Figures 2 through 5 and combinations of Eqns. A3 through A9 (see Appendix 1). Results of these calculations are presented in Table 4 except U_i values with large uncertainties based on imprecise ²⁰⁷Pb*/²³⁵U ages. Values of U_i calculated from the data presented in Figures 4a and 5 range from 4.2 to 17.1 and 2.0 to 17, respectively (Table 4). Values of U_i calculated using equations for temporal evolution of ²³⁰Th/²³⁸U and ²³⁴U/²³⁸U (Eqns. A8 and A9) range from 1.3 to 7.2 (Fig. 3, Table 4). These different estimates of U_i values do not coincide and the ²³⁴U/²³⁸U–²³⁰Th/²³⁸U systematics give the smallest U_i values. Possible reasons of the observed inconsistencies in U_i values are discussed in the following sections.

5. DISCUSSION

5.1. Age Discordance

For an ideal opal sample that formed instantly T years ago with zero initial abundance of all ²³⁸U daughters (except ²³⁴U) and that behaved as a closed system relative to U-series isotopes, all the approaches to age calculations discussed above must give identical values for T. At the same time, the ²⁰⁷Pb*/²³⁵U disequilibrium age (T_{7/5}) and four other ages calculated from ²³⁸U-series isotopes discussed in the previous section are discordant to different degrees (Table 4, Fig. 6). A large discordance is observed between T_{7/5} and the conventional ²⁰⁶Pb*/²³⁸U age (T_{6/8}), with T_{6/8} > T_{7/5} (Table 4, Fig. 6a). This relation can be explained by an excess of radiogenic ²⁰⁶Pb* derived from the initial excess of ²³⁴U. The large age discordance also is observed between T_{7/5} and the ²³⁰Th/U age (T_{0/4}; Fig. 6b). Ages calculated on the basis of ²⁰⁶Pb*/²³⁸U vs. ²³⁴U/²³⁸U (T_{6/4}) and ²⁰⁶Pb*/²³⁸U vs. ²³⁰Th/²³⁸U (T_{6/0}) are much closer to T_{7/5}, but the discordance increases for samples with T_{7/5} greater than 1 My (Fig. 6c,d). Two data points plotting above the Equal Age Line on Figure 6c (samples HD2179Pb1 and HD2079CPb2-1) require the presence in these two samples of ²⁰⁶Pb unsupported by parents ²³⁸U, ²³⁴U, and ²³⁰Th. Similar excess of ²⁰⁶Pb was also found in low U calcites adjacent to opal samples HD2065Pb1, HD2098Pb1, and HD2059Pb3 (L.A. Neymark, Y.V. Amelin, J.B. Paces, unpublished data). The origin of this ²⁰⁶Pb* excess is not completely understood and may be caused by different reasons such as initial radiogenic ²⁰⁶Pb (unlikely due to low Pb solubility in groundwater) or initial excess of radioactive products of ²³⁸U after ²³⁰Th in the U-series decay chain (²²⁶Ra or ²²²Rn). This excess ²⁰⁶Pb* is not likely to be present in smaller amounts in other analyzed opals, because of the observed concordance of T_{7/5} and T_{6/4} ages in most ≤1-Ma-old samples (Fig. 6c).

The general discordance pattern T_{7/5} > T_{6/4} > T_{6/0} > T_{0/4} cannot be easily explained by processes of episodic gain or loss of uranium and its daughter products. Lead or ²²²Rn loss would result in T_{0/4} > T_{7/5} and T_{0/4} > T_{6/4}. Recent episodic uranium mobility would cause subhorizontal trends on the U–Th evo-

Table 3. U–Th–Pb isotope data for Yucca Mountain opals from the ESF tunnel.

| No. | Sample name | Sampling locality | Weight (mg) | U (ppm) | Th (ppb) | Pb (ppb) | Th/U | $^{206}\text{Pb}/^{204}\text{Pb}^b$ | $^{206}\text{Pb}/^{204}\text{Pb}^b$ |
|-----|--------------|-------------------|-------------|---------|----------|----------|----------|-------------------------------------|-------------------------------------|
| 1 | HD2008Pb1 | 2272.0 | 1.058 | 111.8 | 884.3 | 26.99 | 7.9E–03 | 915.4 (1.1) | 2625 (165) |
| 2 | HD2055Pb1 | 2911.2 | 2.502 | 97.10 | 560.9 | 8.853 | 5.8E–03 | 698.8 (0.6) | 1693 (136) |
| 3 | HD2055Pb1a | 2911.2 | 1.020 | 149.5 | 171.0 | ND | 1.1E–03 | ND | ND |
| 4 | HD2055Pb4-1 | 2911.2 | 0.188 | 29.49 | 27.50 | 27.04 | 9.3E–04 | 43.2 (1.0) | 48.2 (15) |
| 5 | HD2055PB4-2 | 2911.2 | 3.291 | 128.8 | 4.365 | 25.98 | 3.4E–05 | 377.4 (0.6) | 402.1 (5.8) |
| 6 | HD2056Pb1 | 2922.9 | 3.518 | 90.39 | 398.9 | 11.76 | 4.4E–03 | 1101 (0.7) | 2328 (100) |
| 7 | HD2056Pb1a | 2922.9 | 1.000 | 99.46 | 66.20 | ND | 6.7E–04 | ND | ND |
| 8 | HD2059Pb3 | 3017.8 | 2.315 | 78.33 | 606.3 | 16.92 | 7.7E–03 | 1639 (0.8) | 1 E4 (225) |
| 9 | HD2059Pb3a | 3017.8 | 0.490 | 82.43 | 208.5 | ND | 2.5E–03 | ND | ND |
| 10 | HD2063Pb1 | 3116.1 | 0.788 | 91.99 | 1187 | 19.21 | 1.3E–02 | 346.3 (1.1) | 590 (72) |
| 11 | HD2065Pb1 | 3316.2 | 0.545 | 236.4 | 858.3 | 33.24 | 3.6E–03 | 572.6 (1.0) | 1581 (155) |
| 12 | HD2065Pb1a | 3316.2 | 0.060 | 312.9 | 372.7 | ND | 1.2E–03 | ND | ND |
| 13 | HD2065Pb2 | 3316.2 | 0.085 | 166.4 | 15.10 | 33.22 | 9.1E–05 | 70.8 (0.9) | 107 (55) |
| 14 | HD2066Pb1-1 | 3395.8 | 1.290 | 136.4 | 1088 | 41.35 | 8.0E–03 | 1046 (1.0) | 1709 (57) |
| 15 | HD2066PB1-2 | 3395.8 | 0.183 | 259.8 | 2556 | 83.26 | 9.8E–03 | 208.9 (1.4) | 286 (37) |
| 16 | HD2066Pb1a | 3395.8 | 1.000 | 292.0 | 3740 | ND | 1.3E–02 | ND | ND |
| 17 | HD2079CPb1 | 3817.2 | 2.022 | 162.7 | 462.7 | 63.64 | 2.8E–03 | 11370 (2.0) | 1.7 75 (1132) |
| 18 | HD2079CPb1a | 3817.2 | 1.180 | 193.7 | 298.6 | ND | 1.5E–03 | ND | ND |
| 19 | HD2079CPb2-1 | 3817.2 | 0.447 | 121.7 | 249.7 | 69.02 | 2.1E–03 | 717 (3.1) | 1072 (41) |
| 20 | HD2079CPb2-2 | 3817.2 | 0.916 | 160.1 | <5 | 71.25 | <3.1E–05 | 1224 (0.6) | 1679 (30) |
| 21 | HD2079CPb2-3 | 3817.2 | 0.383 | 123.1 | 4.958 | 52.32 | 4.0E–05 | 545.3 (0.5) | 901 (54) |
| 22 | HD2098Pb1 | 2678.1 | 0.463 | 182.0 | 1010 | 14.98 | 5.6E–03 | 53.3 (0.4) | 55 (19) |
| 23 | HD2098Pb1a | 2678.1 | 0.070 | 126.1 | 546.0 | ND | 4.3E–03 | ND | ND |
| 24 | HD2098Pb2 | 2678.1 | 0.033 | 236.5 | <140 | 43.72 | <5.9E–04 | 24.0 (0.5) | 22 (15) |
| 25 | HD2100Pb1 | 4026.9 | 2.609 | 140.6 | 537.9 | 40.47 | 3.8E–03 | 6576 (0.7) | 18951 (157) |
| 26 | HD2100Pb1a | 4026.9 | 0.460 | 169.6 | 260.4 | ND | 1.5E–03 | ND | ND |
| 27 | HD2168Pb1 | 5771.7 | 0.711 | 95.44 | 6.940 | 73.89 | 7.3E–05 | 1186 (0.5) | 1766 (40) |
| 28 | HD2179Pb1 | 6320.2 | 0.465 | 81.90 | 7.551 | 70.35 | 9.2E–05 | 580.6 (0.6) | 793 (30) |
| 29 | HD2179Pb2-1 | 6320.2 | 1.656 | 112.6 | 14.43 | 34.73 | 1.3E–04 | 1604 (1.2) | 2687 (55) |
| 30 | HD217-Pb2-2 | 6320.2 | 0.151 | 54.98 | 332.1 | 17.16 | 6.0E–03 | 57.74 (0.5) | 81 (48) |
| 31 | HD2179Pb2-3 | 6320.2 | 0.801 | 56.08 | 2.99 | 13.66 | 5.3E–05 | 209.8 (0.3) | 289 (34) |
| 32 | HD2181APb1 | 6338.1 | 0.807 | 99.09 | 0.745 | 35.07 | 7.5E–06 | 421.8 (0.4) | 530 (23) |
| 33 | HD2277Pb1 | 7681.0 | 3.252 | 75.23 | 20.42 | 28.33 | 2.7E–04 | 266.3 (0.6) | 277.4 (3.9) |
| 34 | HD2281Pb1 | 7806.4 | 0.811 | 39.72 | 6.658 | 14.06 | 1.7E–04 | 323.6 (1.0) | 542 (58) |
| 35 | HD2283Pb1 | 7990.0 | 1.077 | 130.5 | 545.2 | 48.08 | 4.2E–03 | 1920 (1.0) | 4146 (94) |

^a Distance in meters from the sampling site to the north portal of the ESF tunnel.

^b Measured isotopic ratio. Here and throughout the table numbers in parentheses are relative errors in percent.

^c Isotopic ratios, corrected for fractionation, spike contribution, and procedure blank.

^d Activity ratios, calculated from measured isotopic ratios corrected for fractionation, spike contribution, and procedure blank.

^e Pb/U ratios, corrected for fractionation, spike, blank, and initial common lead.

^f Error correlation between $^{207}\text{Pb}/^{235}\text{U}$ and $^{206}\text{Pb}/^{238}\text{U}$.

All data are corrected for common Pb using average YM calcite and water values: $^{206}\text{Pb}/^{204}\text{Pb} = 18.83 \pm 0.82$, $^{207}\text{Pb}/^{204}\text{Pb} = 15.62 \pm 0.09$, $^{208}\text{Pb}/^{204}\text{Pb} = 38.78 \pm 0.53$.

Blank values $^{206}\text{Pb}/^{204}\text{Pb} = 17.95 (\pm 8.5\%)$, $^{207}\text{Pb}/^{204}\text{Pb} = 15.31 (\pm 6.9\%)$, $^{208}\text{Pb}/^{204}\text{Pb} = 36.68 (\pm 7.6\%)$.

Rho ($^{206}\text{Pb}/^{204}\text{Pb} - ^{207}\text{Pb}/^{204}\text{Pb}$) = 0.8, [Pb] = 1.5 pg ($\pm 80\%$), [U] = 1 pg ($\pm 80\%$).

ND, not determined.

lution diagram (Fig. 3) and a calculated excess of ^{230}Th unsupported by uranium should be observed at least in some cases for samples with the oldest $^{230}\text{Th}/\text{U}$ ages. The data do not have any of these features. In addition, for 10 opal samples with the most precise $T_{7/5}$ ages in the range between 170 and 859 ka (Table 4), these values are concordant with $T_{6/4}$ ages within error limits, which may indicate closed system behavior for U and its daughters in these 10 samples. At the same time, in 4 of these 10 cases where $^{230}\text{Th}/\text{U}$ ages ($T_{0/4}$) were measured in the same sample digestions using the U–Th–Pb mixed spike, the $T_{0/4}$ values are systematically younger than corresponding U–Pb ages (Table 4). Any process of episodic gain or loss in the uranium decay chain cannot explain this age discordance.

The observed age discordance pattern matches better a model of continuous uranium additions to the opals as it was suggested for U-series results in fossil bones and corals

(Bischoff et al., 1995; Cheng et al., 1999) and for water–rock interaction processes (Scott et al., 1992). Continuous U gain will cause U–Pb ages to be systematically older than $^{230}\text{Th}/\text{U}$ ages, because ages based on shorter-lived isotopes are nonlinearly biased to younger values by recent uranium additions. However, in the case of Yucca Mountain opals, the hypothesized process of continuous U gain does not necessarily mean uranium migration under open system conditions. The observed age discordance rather conflicts with common age interpretations that assume that the analyzed samples consist of materials instantaneously deposited during discrete episodes. The age discordance can be explained by slow mineral growth as described in the Neymark and Paces (2000) model of continuous deposition proposed for interpretation of previous $^{230}\text{Th}/\text{U}$ dating results of Yucca Mountain opals. This hypothetical model is mathematically equivalent to a continuous uranium gain

Table 3. (Continued)

| $^{206}\text{Pb}/^{207}\text{Pb}^b$ | $^{206}\text{Pb}/^{208}\text{Pb}^b$ | $^{206}\text{Pb}^*/^{238}\text{U}^c$ | $^{207}\text{Pb}^*/^{235}\text{U}^e$ | Rho ^f 6/8–7/5 | $^{207}\text{Pb}^*/^{206}\text{Pb}^{a,e}$ | $^{238}\text{U}/^{204}\text{Pb}^c$ | $^{232}\text{Th}/^{230}\text{Th}_{\text{act}}^d$ | $^{234}\text{U}/^{238}\text{U}_{\text{act}}^d$ | $^{230}\text{Th}/^{238}\text{U}_{\text{act}}^d$ |
|-------------------------------------|-------------------------------------|--------------------------------------|--------------------------------------|-----------------------------|---|------------------------------------|--|--|---|
| 36.11 | 41.37 | 0.0002651 (1.2) | 0.000800 (7.9) | 0.32 | 0.0219 (3.8) | 9.83E+06 | ND | 1.283 (0.65) | ND |
| 55.71 | 40.19 | 0.0001005 (1.5) | 0.000122 (25) | 0.16 | 0.0171 (2.3) | 2.59E+07 | ND | 4.132 (0.56) | ND |
| ND | ND | ND | ND | ND | ND | ND | 1.24E–06 | 4.798 (0.48) | 2.295 (0.44) |
| 3.046 | 1.267 | 0.000303 (9.1) | 0.00028 (198) | 0.25 | 0.007 (196) | 9.69E+04 | 8.45E–05 | 4.541 (0.89) | 3.520 (0.86) |
| 20.12 | 10.40 | 0.0001947 (0.47) | 0.000306 (3.1) | 0.40 | 0.0114 (3.0) | 1.97E+06 | 3.91E–06 | 2.926 (0.35) | 2.765 (0.41) |
| 59.18 | 48.37 | 0.0001447 (0.83) | 0.000205 (11) | 0.23 | 0.0103 (5.6) | 1.60E+07 | ND | 3.941 (0.42) | ND |
| ND | ND | ND | ND | ND | ND | ND | 6.37E–05 | 3.893 (0.49) | 3.331 (0.51) |
| 99.58 | 167.1 | 0.0002470 (0.43) | 0.000290 (7.0) | 0.23 | 0.0085 (7.0) | 4.09E+07 | ND | 3.101 (0.44) | ND |
| ND | ND | ND | ND | ND | ND | ND | 2.97E–04 | 2.938 (0.54) | 2.719 (0.48) |
| 29.33 | 14.58 | 0.0002130 (2.3) | 0.00023 (45) | 0.20 | 0.0079 (22) | 2.68E+06 | ND | 4.694 (0.77) | ND |
| 57.37 | 38.36 | 0.0001549 (1.8) | 0.00016 (35) | 0.24 | 0.0076 (35) | 1.01E+07 | ND | 5.481 (0.38) | ND |
| ND | ND | ND | ND | ND | ND | ND | 1.27E–04 | 6.179 (0.79) | 2.982 (1.1) |
| 6.745 | 2.813 | 0.000126 (11) | 0.00005 (390) | 0.13 | 0.0027 (390) | 6.98E+05 | 8.04E–06 | 5.696 (0.49) | 3.600 (0.43) |
| 46.43 | 47.59 | 0.0003345 (0.65) | 0.000578 (7.4) | 0.26 | 0.0125 (3.6) | 5.05E+06 | ND | 2.707 (0.39) | ND |
| 15.53 | 7.319 | 0.0002890 (2.6) | 0.00042 (39) | 0.27 | 0.010 (19) | 9.24E+05 | ND | 3.442 (0.83) | ND |
| ND | ND | ND | ND | ND | ND | ND | 1.48E–03 | 2.729 (0.55) | 2.760 (2.2) |
| 106.7 | 1153 | 0.0004508 (0.33) | 0.000577 (2.0) | 0.23 | 0.0093 (1.9) | 3.72E+08 | ND | 2.409 (0.32) | ND |
| ND | ND | ND | ND | ND | ND | ND | 1.91E–04 | 2.562 (0.55) | 2.573 (0.43) |
| 48.79 | 30.58 | 0.0006151 (0.76) | 0.00051 (15) | 0.20 | 0.0060 (15) | 1.71E+06 | 2.65E–04 | 2.298 (0.62) | 2.466 (3.5) |
| 43.59 | 42.62 | 0.0004892 (0.47) | 0.000931 (2.0) | 0.31 | 0.0138 (2) | 3.39E+06 | 0.00E+00 | 1.618 (0.59) | 1.827 (0.38) |
| 29.56 | 23.03 | 0.0004492 (1.2) | 0.00104 (5.3) | 0.31 | 0.0169 (5) | 1.96E+06 | 6.68E–06 | 1.685 (0.67) | 1.92 (11) |
| 3.436 | 1.479 | 0.0000316 (9.5) | 0.000049 (185) | 0.34 | 0.011 (91) | 1.15E+06 | ND | 5.565 (0.44) | ND |
| ND | ND | ND | ND | ND | ND | ND | 4.43E–04 | 5.370 (0.80) | 3.117 (1.3) |
| 1.412 | 0.567 | 0.0000093 (61) | 0.00004 (742) | 0.51 | 0.03 (713) | 3.65E+05 | 0.00E+00 | 6.066 (0.50) | 1.697 (1.4) |
| 60.79 | 278.5 | 0.0003281 (0.57) | 0.000771 (1.6) | 0.41 | 0.02 (705) | 5.77E+07 | ND | 1.645 (1.2) | ND |
| ND | ND | ND | ND | ND | ND | ND | 2.61E–04 | 1.656 (0.54) | 1.873 (0.48) |
| 42.94 | 32.26 | 0.0008449 (0.49) | 0.00170 (2.3) | 0.30 | 0.0146 (2.2) | 2.07E+06 | 2.04E–05 | 1.124 (0.60) | 1.136 (0.56) |
| 45.22 | 9.556 | 0.0008646 (0.77) | 0.000295 (24) | 0.14 | 0.0025 (24) | 8.95E+05 | 1.29E–05 | 2.591 (0.48) | 2.283 (0.85) |
| 33.34 | 58.32 | 0.0003404 (0.49) | 0.001143 (1.4) | 0.43 | 0.0243 (1.3) | 7.84E+06 | 2.90E–05 | 1.423 (0.30) | 1.412 (0.48) |
| 4.97 | 2.10 | 0.000165 (13) | 0.00028 (111) | 0.22 | 0.01 (109) | 3.80E+05 | 8.51E–04 | 2.645 (0.77) | 2.265 (2.23) |
| 15.67 | 6.91 | 0.000218 (2.29) | 0.000319 (18) | 0.24 | 0.011 (18) | 1.24E+06 | 7.56E–06 | 2.518 (0.44) | 2.249 (0.80) |
| 19.78 | 14.15 | 0.0003537 (0.89) | 0.001093 (3.2) | 0.38 | 0.0224 (3.0) | 1.47E+06 | 1.82E–06 | 1.349 (0.93) | 1.316 (0.49) |
| 13.97 | 6.709 | 0.0003333 (0.51) | 0.000752 (3.7) | 0.46 | 0.0164 (3.4) | 7.76E+05 | 5.25E–05 | 1.547 (0.41) | 1.648 (0.33) |
| 26.09 | 12.54 | 0.0003548 (2.0) | 0.00048 (17) | 0.22 | 0.01 (17) | 1.47E+06 | 4.07E–05 | 3.342 (0.30) | 1.314 (0.88) |
| 34.98 | 75.37 | 0.0004096 (0.50) | 0.001408 (1.4) | 0.43 | 0.0249 (1.3) | 1.01E+07 | 1.21E–03 | 1.117 (0.37) | 1.102 (3.9) |

model, but assumes that the opal deposition proceeds at very slow but uniform rates such that all samples of finite thickness will integrate multiple, infinitely thin layers with continuously varying age. After deposition each of these layers behaves as a closed system with regard to uranium and its decay products. Resulting isotopic measurements will represent mixtures of multiage materials intermediate between the oldest and the youngest layers. The model predicts differences in calculated conventional ages when finely laminated minerals are mechanically mixed during sampling, favoring older ages for the isotopic system based on a longer half-life of the isotope involved in age calculations. The general form of the integral equations of the model of continuous deposition, assuming that the sample studied consisted of an infinite number of infinitely thin layers, is (Neymark and Paces, 2000):

$$(D/P)_t = \int_0^t D(t)dt / \int_0^t P(t)dt, \quad (1)$$

where D and P denote daughter and parent isotopes and $t = 0$ the start of deposition.

Eqn. 1 was used to simulate time-integrated isotope ratios for $^{206}\text{Pb}/^{238}\text{U}$, $^{207}\text{Pb}/^{235}\text{U}$, $^{230}\text{Th}/^{238}\text{U}$, $^{231}\text{Pa}/^{235}\text{U}$, ^{14}C , and $^{226}\text{Ra}/^{230}\text{Th}$, in order of decreasing half-lives, assuming con-

stant concentration of P at the time of deposition, constant depositional rate, and zero age of the outermost layer. Comparisons between the true average ages (half the total duration of deposition) and apparent average ages determined using these simulated isotope ratios based on continuous deposition and the conventional age equations indicate that all calculated ages (excluding $^{207}\text{Pb}/^{235}\text{U}$) are younger than the true average ages (Fig. 7a). Apparent average ages calculated using conventional age equations are nonlinear functions of the true average ages (Fig. 7a) because of the exponential terms associated with the law of radioactive decay. These ages most closely equate to true average ages (data points plot on the equal age line; Fig. 7a) at the youngest end of the working age range for each isotopic system involving short-lived isotopes. Calculated apparent ages diverge significantly from the equal age line at the older end of the working-age range, but fail to ever reach the upper limits of the geochronometer because of the small amounts of young material present on the outermost surface of the mineral. Therefore, in the case of slow continuous deposition, conventional apparent ages may significantly misrepresent the true average age of the sample analyzed.

The model calculations presented in Figure 7a show that $^{207}\text{Pb}/^{235}\text{U}$ ($T_{7/5}$) ages are practically equal to the true average ages of the mixed layer, whereas $^{206}\text{Pb}^*/^{238}\text{U}$ – $^{234}\text{U}/^{238}\text{U}$

Table 4. Calculated U–Th–Pb ages (ka) and $^{234}\text{U}/^{238}\text{U}$ initial activity ratios for Yucca Mountain opals.

| No | Sample name | $^{206}\text{Pb}^*/^{238}\text{U}$ age ^a | $^{207}\text{Pb}^*/^{235}\text{U}$ age ^a | $^{207}\text{Pb}^*/^{235}\text{U}$ age ^b | $^{234}\text{U}/^{238}\text{U}$ age ^c | $^{234}\text{U}/^{238}\text{U}$ age ^d | $^{206}\text{Pb}/^{234}\text{U}$ age ^e | $^{234}\text{U}/^{238}\text{U}$ age ^f | $^{206}\text{Pb}/^{230}\text{Th}$ age ^g | $^{234}\text{U}/^{238}\text{U}$ age ^h | $^{230}\text{Th}/^{238}\text{U}$ age ⁱ | $^{234}\text{U}/^{238}\text{U}$ age ^j |
|----|--------------|---|---|---|--|--|---|--|--|--|---|--|
| 1 | HD2008Pb1 | 1708 ± 20 | 812 ± 64 | 859 ± 64 | 4.12 ± 0.59 | 4.23 ± 0.59 | 851 ± 12 | 4.155 ± 0.093 | ND | ND | ND | ND |
| 2 | HD2005Pb1 | 648 ± 10 | 124 ± 31 | 170 ± 32 | 9.2 ± 2.9 | 6.07 ± 0.46 | 211.4 ± 1.6 | 6.701 ± 0.042 | ND | ND | ND | ND |
| 3 | HD2005Pb1a | ND | ND | ND | ND | ND | ND | ND | ND | ND | ND | ND |
| 4 | HD2005Pb4-1 | 1952 ± 177 | 288 ± 570 | 335 ± 570 | 12 ± *** | 10 ± 15 | 359 ± 24 | 10.81 ± 0.11 | 372 ± 31 | 11.174 ± 0.041 | 64.5 ± 0.5 | 5.561 ± 0.023 |
| 5 | HD2005Pb4-2 | 1255 ± 6 | 310.3 ± 9.8 | 357 ± 10 | 6.83 ± 0.25 | 6.30 ± 0.15 | 372.0 ± 0.6 | 6.526 ± 0.029 | 322.9 ± 1.3 | 5.808 ± 0.027 | 131.0 ± 2.7 | 6.002 ± 0.039 |
| 6 | HD2005Pb1 | 933 ± 8 | 208 | 255 ± 24 | 7.5 ± 1.0 | 7.1 ± 0.4 | 264.2 ± 1.1 | 7.217 ± 0.035 | ND | ND | 188.1 ± 2.2 | 4.282 ± 0.016 |
| 7 | HD2005Pb1a | ND | ND | ND | ND | ND | ND | ND | ND | ND | ND | ND |
| 8 | HD2005Pb3 | 1592 ± 14 | 294 ± 42 | 341 ± 42 | 9.3 ± 1.3 | 6.52 ± 0.66 | 406.7 ± 2.2 | 7.653 ± 0.043 | ND | ND | 151.0 ± 1.9 | 5.438 ± 0.021 |
| 9 | HD2009Pb3a | ND | ND | ND | ND | ND | ND | ND | ND | ND | 180.0 ± 2.8 | 4.229 ± 0.018 |
| 10 | HD2006Pb1 | 1373 ± 32 | 234 ± 104 | 281 ± 110 | 10 ± 7 | 9.2 ± 2.6 | 292.8 ± 4.1 | 9.469 ± 0.082 | ND | ND | ND | ND |
| 11 | HD2006Pb1 | 998 | 166 ± 58 | 212 ± 59 | 10 ± 5 | 9.2 ± 1.4 | 226.0 ± 2.3 | 9.503 ± 0.037 | ND | ND | ND | ND |
| 12 | HD2005Pb1a | ND | ND | ND | ND | ND | ND | ND | ND | ND | ND | ND |
| 13 | HD2005Pb2 | 814 ± 89 | 48 ± 188 | 88 ± 188 | 33 ± *** | 7.0 ± 3.2 | 198 ± 12 | 9.235 ± 0.049 | 193 ± 14 | 9.11 ± 0.34 | 64.9 ± 1.1 | 7.226 ± 0.050 |
| 14 | HD2006Pb1-1 | 2156 ± 14 | 587 ± 43 | 634 ± 43 | 7.09 ± 0.45 | 11.3 ± 1.3 | 518.4 ± 2.1 | 8.418 ± 0.045 | ND | ND | 92.78 ± 0.85 | 7.108 ± 0.027 |
| 15 | HD2006Pb1-2 | 1863 ± 48 | 423 ± 166 | 470 ± 170 | 8 ± 4 | 10.3 ± 4.5 | 413.7 ± 7.9 | 8.888 ± 0.091 | ND | ND | ND | ND |
| 16 | HD2006Pb1a | ND | ND | ND | ND | ND | ND | ND | ND | ND | 222 ± 13 | 4.25 ± 0.12 |
| 17 | HD2079CPb1 | 2905 ± 10 | 585 ± 12 | 632 ± 32 | 9.91 ± 0.18 | 9.45 ± 0.29 | 645.0 ± 2.0 | 9.764 ± 0.046 | ND | ND | ND | ND |
| 18 | HD2079CPb1a | ND | ND | ND | ND | ND | ND | ND | ND | ND | 221.0 ± 4.0 | 3.922 ± 0.019 |
| 19 | HD2079CPb2-1 | 3964 ± 30 | 519 ± 77 | 566 ± 77 | 15.0 ± 1.7 | 7.5 ± 1.4 | 762.8 ± 5.2 | 12.27 ± 0.12 | 671 ± 13 | 9.69 ± 0.33 | 274 ± 31 | 3.82 ± 0.24 |
| 20 | HD2079CPb2-2 | 3153 ± 15 | 944 ± 19 | 991 ± 19 | 8.06 ± 0.14 | 11.25 ± 0.57 | 887 ± 14 | 8.64 ± 0.12 | 686 ± 9 | 5.32 ± 0.12 | 452 ± 32 | 3.22 ± 0.17 |
| 21 | HD2079CPb2-3 | 2895 ± 33 | 1059 ± 56 | 1106 ± 56 | 6.75 ± 0.33 | 16.7 ± 2.5 | 828.6 ± 5.3 | 8.17 ± 0.12 | 643 ± 19 | 5.24 ± 0.24 | 465 ^{+ini/-200} | 3.6 ± 3.3 |
| 22 | HD2098Pb1 | 204 ± 19 | 50 ± 92 | 90 ± 90 | 8 ± *** | 6.9 ± 1.5 | 97.7 ± 3.7 | 7.021 ± 0.032 | ND | ND | ND | ND |
| 23 | HD2098Pb1a | ND | ND | ND | ND | ND | ND | ND | ND | ND | 82.7 ± 1.7 | 6.528 ± 0.046 |
| 24 | HD2098Pb2 | 60 ± 36 | 45 ± 335 | 84 ± 335 | 3 ± *** | 7.4 ± 6.1 | 50.1 ± 9.1 | 6.839 ± 0.035 | 39 ± 14 | 6.65 ± 0.23 | 34.1 ± 0.6 | 6.580 ± 0.032 |
| 25 | HD2100Pb1 | 2115 ± 12 | 718 ± 12 | 829 ± 12 | 5.60 ± 0.10 | 7.76 ± 0.31 | 734 ± 19 | 6.162 | ND | ND | ND | ND |
| 26 | HD2100Pb1a | ND | ND | ND | ND | ND | ND | ND | ND | ND | 439 ± 28 | 3.28 ± 0.16 |
| 27 | HD2168Pb1 | 5445 ± 27 | 1725 ± 40 | 1772 ± 40 | 11.83 ± 0.20 | 19.9 ± 2.4 | 1595 ± 285 | 12.42 ± 0.62 | 1021 ± 30 | 3.24 ± 0.20 | 389 ± 31 | 1.373 ± 0.020 |
| 28 | HD2179Pb1 | 5571 ± 43 | 299 ± 71 | 346 ± 71 | 33 ± 8 | 5.24 ± 0.85 | 816.7 ± 4.6 | 17.10 ± 0.13 | 807 ± 23 | 16.7 ± 1.1 | 166.1 ± 3.2 | 3.547 ± 0.021 |
| 29 | HD2179Pb2 | 2194 ± 11 | 1160 ± 16 | 1207 ± 16 | 4.27 ± 0.09 | 13.94 ± 0.60 | 852.0 ± 5.1 | 5.732 ± 0.047 | 643.3 ± 7.3 | 3.620 ± 0.056 | 265.9 ± 5.6 | 1.899 ± 0.011 |
| 30 | HD2179Pb2-2 | 1062 ± 141 | 282 ± 313 | 329 ± ^b | 8 ± ^b | 4.7 ± 3.2 | 363 ± 36 | 5.605 ± 0.057 | 328 ± 50 | 5.16 ± 0.63 | 156.8 ± 6.9 | 3.566 ± 0.050 |
| 31 | HD2179Pb2-3 | 1407 ± 32 | 324 ± 59 | 371 ± 59 | 8.6 ± 2.1 | 4.80 ± 0.64 | 436.3 ± 8.0 | 6.227 ± 0.038 | 396 ± 14 | 3.47 ± 0.10 | 171.2 ± 3.2 | 3.466 ± 0.020 |
| 32 | HD2181APb1 | 2280 ± 20 | 1109 ± 35 | 1156 ± 35 | 4.70 ± 0.19 | 10.23 ± 0.97 | 917 ± 28 | 5.68 ± 0.17 | 676 ± 15 | 3.36 ± 0.10 | 260 ± 11 | 1.729 ± 0.009 |
| 33 | HD2274Pb1 | 2149 ± 11 | 763 ± 28 | 810 ± 28 | 5.81 ± 0.19 | 6.42 ± 0.44 | 780.2 ± 5.9 | 5.986 ± 0.057 | 594.0 ± 6.6 | 3.943 ± 0.058 | 332.2 ± 9.3 | 2.402 ± 0.025 |
| 34 | HD2281Pb1 | 2287 ± 46 | 488 ± 84 | 535 ± 84 | 8.7 ± 1.4 | 11.7 ± 2.5 | 467.9 ± 8.2 | 9.820 ± 0.038 | 677 ± 14 | 16.95 ± 0.64 | 51.08 ± 0.57 | 3.707 ± 0.011 |
| 35 | HD2283Pb1 | 2640 ± 13 | 1429 ± 20 | 1476 ± 20 | 4.70 ± 0.10 | 8.68 ± 0.51 | 1276 ± 43 | 5.35 ± 0.15 | 775 ± 12 | 2.054 ± 0.038 | 333 ^{+120/-60} | 1.301 ± 0.065 |

^a Conventional U–Pb ages calculated assuming initial radioactive equilibrium.^b $^{207}\text{Pb}^*/^{235}\text{U}$ disequilibrium age calculated assuming zero initial activity of ^{231}Pa and ^{227}Ac .^c Initial activity ratio calculated from $^{207}\text{Pb}^*/^{235}\text{U}$ disequilibrium age and measured $^{206}\text{Pb}^*/^{238}\text{U}$ assuming closed system behavior.^d Initial activity ratio calculated from $^{207}\text{Pb}^*/^{235}\text{U}$ disequilibrium age and measured $^{234}\text{U}/^{238}\text{U}$ assuming closed system behavior.^e Calculated from measured $^{206}\text{Pb}^*/^{238}\text{U}$ and $^{234}\text{U}/^{238}\text{U}$.^f Calculated from measured $^{206}\text{Pb}^*/^{238}\text{U}$ and $^{230}\text{Th}/^{238}\text{U}$.^g Calculated from measured $^{230}\text{Th}/^{238}\text{U}$ and $^{234}\text{U}/^{238}\text{U}$ activity ratios.^h Error exceeds 100% of the value.

ND, not determined.

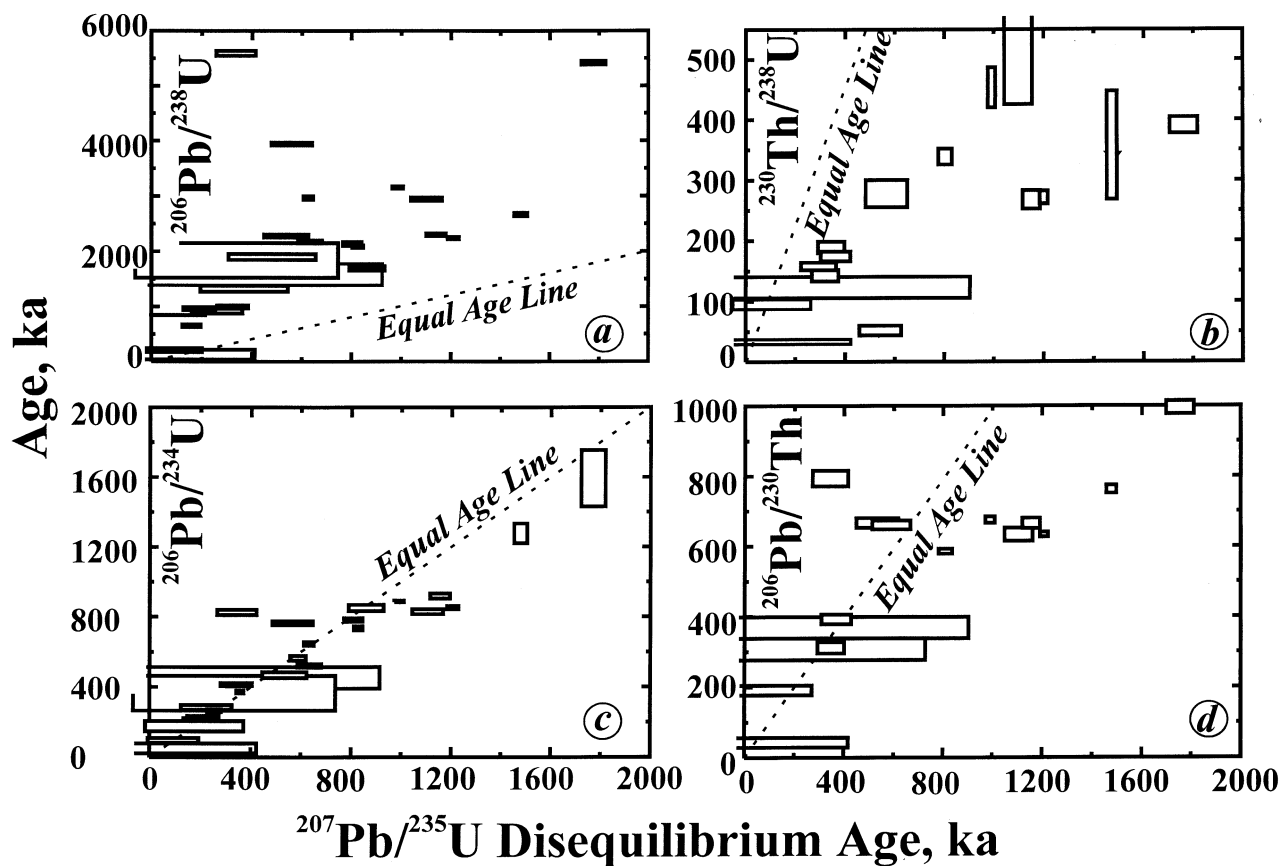


Fig. 6. A comparison between different U–Th–Pb ages for Yucca Mountain opals. All the ages are plotted against the $^{207}\text{Pb}/^{235}\text{U}$ disequilibrium age ($T_{7/5}$). (a) Conventional $^{206}\text{Pb}/^{238}\text{U}$ age ($T_{6/8}$) is systematically larger than $T_{7/5}$ reflecting an initial excess of ^{234}U . (b) Conventional $^{230}\text{Th}/^{234}\text{U}$ age ($T_{0/4}$) is systematically smaller than $T_{7/5}$. Ages shown in (c) and (d) are obtained by using the new concordia diagrams (Fig. 4a and 5). These ages are less discordant with $T_{7/5}$ than $T_{6/8}$ and $T_{0/4}$. Note differences in the y-axis scales.

($T_{6/4}$), $^{206}\text{Pb}^*/^{238}\text{U}$ – $^{230}\text{Th}/^{238}\text{U}$ ($T_{6/0}$), and $^{230}\text{Th}/^{238}\text{U}$ – $^{234}\text{U}/^{238}\text{U}$ ($T_{0/4}$) ages are biased to younger values because they are more dependent on the decay of ^{234}U and ^{230}Th , which have much shorter half-lives than ^{238}U and ^{235}U . All the values are much less discordant when young ages are calculated (Table 4) and this is not a result of larger relative errors, because this relation also holds for most precise age results. The distributions of U–Pb and previously obtained $^{230}\text{Th}/\text{U}$ (opal and calcite) and ^{14}C (calcite) ages for outermost surfaces of Yucca Mountain low-temperature fracture- and cavity-coating minerals (Fig. 7b) reasonably follow predictions of the model of continuous deposition (U/Pb age > $^{230}\text{Th}/\text{U}$ age > ^{14}C age).

A closer look at the discordance between $T_{6/4}$ and $T_{0/4}$ ages (Fig. 8) shows that consistency with an ideal model of continuous deposition with a constant rate until present is not perfect. All the data confirm the general pattern of $T_{6/4} > T_{0/4}$ and about half of the data points do plot within the $U_i = 2$ and $U_i = 10$ boundaries predicted by the continuous deposition model for different $^{234}\text{U}/^{238}\text{U}$ initial activity ratios (U_i). However, some samples plot above the model curves requiring a non-zero age of the outermost mineral surface and others plot below the model curves requiring the presence of excess ^{206}Pb unsupported by ^{234}U . The data presented in Figure 8 also demonstrate that there are no systematic differences between the results

obtained for aliquots analyzed separately for U–Pb and $^{230}\text{Th}/\text{U}$ and those for single sample digests analyzed with a mixed U–Th–Pb spike.

5.2. Initial $^{234}\text{U}/^{238}\text{U}$ Ratios

Initial $^{234}\text{U}/^{238}\text{U}$ ratios calculated from U–Th–Pb isotopic data can be used to interpret the origin of infiltrating solutions and the processes of percolation through the UZ because the uranium isotopic composition of percolating water at the time of mineral deposition is preserved in the solid phase. If the mineral experiences no changes in the abundances of nuclides other than through radioactive decay, this same ratio will be calculated from the measured $^{234}\text{U}/^{238}\text{U}$, $^{230}\text{Th}/^{238}\text{U}$, and $^{206}\text{Pb}^*/^{238}\text{U}$. However, most $^{234}\text{U}/^{238}\text{U}$ initial activity ratios (U_i) for a given sample calculated by different methods are discordant (Table 4). Values of U_i calculated from (1) measured $^{234}\text{U}/^{238}\text{U}$ and $^{230}\text{Th}/^{238}\text{U}$ (y-intercepts of corresponding evolution curves on Fig. 3) and (2) measured $^{234}\text{U}/^{238}\text{U}$ and $^{207}\text{Pb}^*/^{235}\text{U}$ (y-intercepts on Fig. 4b) are shown in Figure 9a,b, where they are plotted against $T_{7/5}$ age. A simplistic interpretation of the negative correlation between U_i and $T_{7/5}$ in Figure 9a would require a monotonic decrease in groundwater $^{234}\text{U}/^{238}\text{U}$ ratio with increasing age. At the same time, U_i calculated

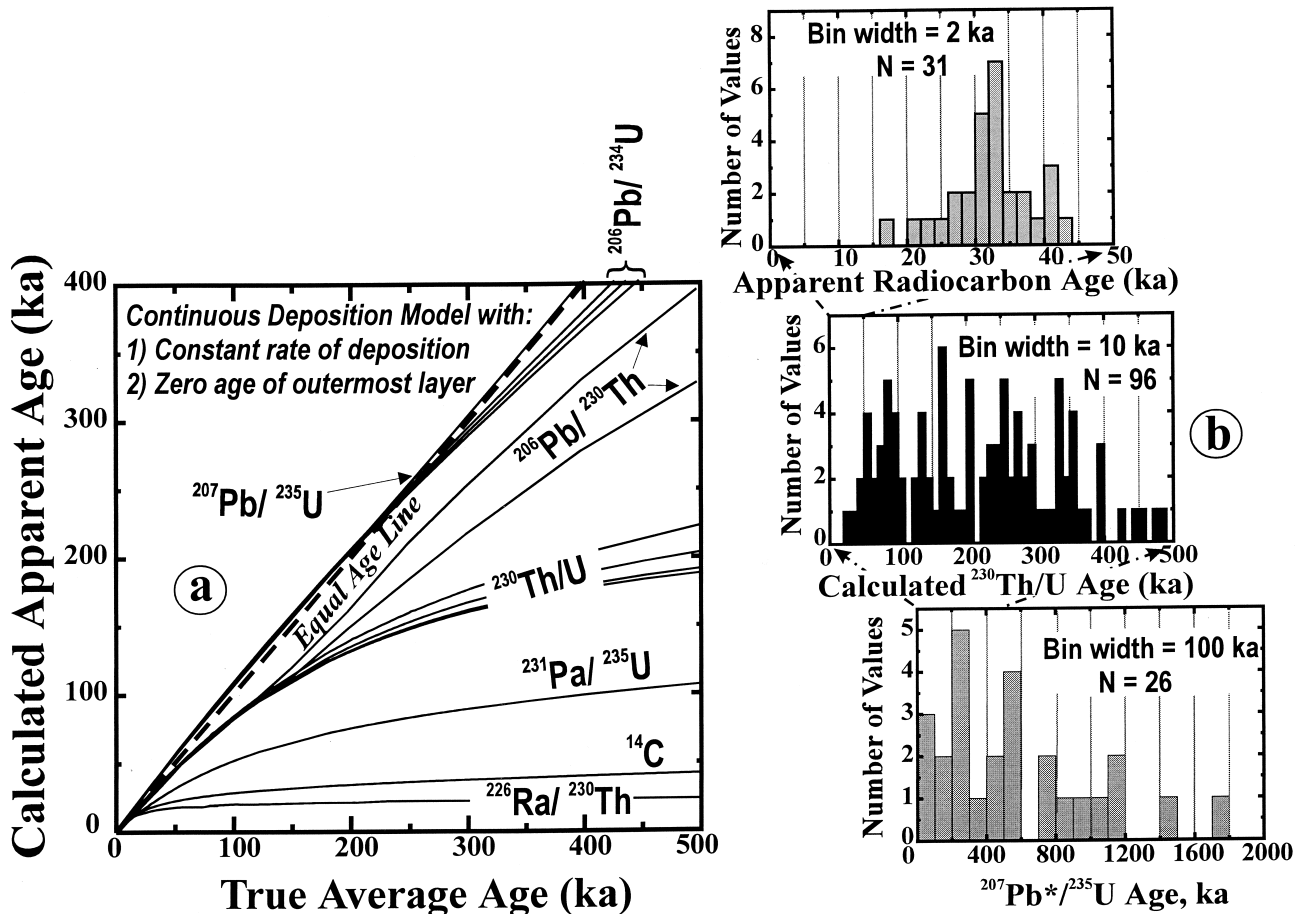


Fig. 7. (a) Relations between calculated ages and the true average age of deposition for an integrated multiage sample collected from the outermost surface of a mineral continuously deposited with a constant rate and having a zero-age outermost surface. This continuous deposition model (Neymark and Paces, 2000) predicts the following general age discordance pattern for multiage opal samples: $T_{7/5} > T_{6/4} > T_{6/0} > T_{0/4} > {}^{231}\text{Pa}/{}^{235}\text{U}$ age $>$ Radiocarbon age (for associated calcite) $>$ ${}^{226}\text{Ra}/{}^{230}\text{Th}$ age. For $T_{6/4}$, $T_{6/0}$, and $T_{0/4}$, two curves shown correspond to $U_i = 2$ (upper curve in each case) and $U_i = 10$. (b) Histograms showing distributions of radiocarbon ${}^{230}\text{Th}/\text{U}$ (Paces et al., 1998a), and ${}^{207}\text{Pb}/{}^{235}\text{U}$ (this work) ages in Yucca Mountain fracture- and cavity-filling calcites and opals. Note differences in the scales for the abscissas for different histograms.

from Figure 4b is positively correlated with ${}^{207}\text{Pb}/{}^{235}\text{U}$ age (Fig. 9b). In addition, U_i ratios larger than 10 were not observed for Yucca Mountain groundwater (Paces et al., 1998b). These contradictions mean that the observed correlations do not reflect real temporal variations of ${}^{234}\text{U}/{}^{238}\text{U}$ ratio in groundwater. Again, as discussed above for the case of the age discordance, the data points (with two exceptions, samples HD2179Pb1 and HD2079CPb2-1) plot within the boundaries $U_i = 2$ and $U_i = 10$ predicted by the model of continuous deposition (Fig. 9a,b). These results also support the concept that the analyzed subsamples of the outermost surface of coatings consisted of multiage materials and demonstrate that ${}^{230}\text{Th}/\text{U}$ data give biased estimates for ages and ${}^{234}\text{U}/{}^{238}\text{U}$ initial activity ratios.

5.3. Rates of Deposition and Implications for the Site Paleohydrology

The obtained ages demonstrate that low-temperature secondary mineral deposition within Yucca Mountain is a long-term

process that has been active for most of the Quaternary. These data also allow evaluation of long-term rates of deposition in the unsaturated zone. Assuming that the ${}^{207}\text{Pb}/{}^{235}\text{U}$ age ($T_{7/5}$) accurately reflects the average age of continuously deposited opals, and estimates of total sample thickness are realistic, rates of deposition can be calculated. Although quantitative estimates of the subsample thickness are not available, thin sheets sampled from mineral surfaces commonly were 0.1- to 0.3-mm thick. In these cases, deposition rates between about 0.035 and 1.8 mm/m.yr are obtained by dividing the thickness by the total duration of deposition (doubled $T_{7/5}$ from Table 4). These values are in general agreement with long-term rates of mineral deposition during the past 10 m.yr based on direct U–Pb dating of sequential inner layers of opal from calcite–silica fracture and cavity coatings at Yucca Mountain (Neymark et al., 1998a).

Geochronologic information obtained from the opals is useful for interpreting UZ groundwater paleofluxes at Yucca

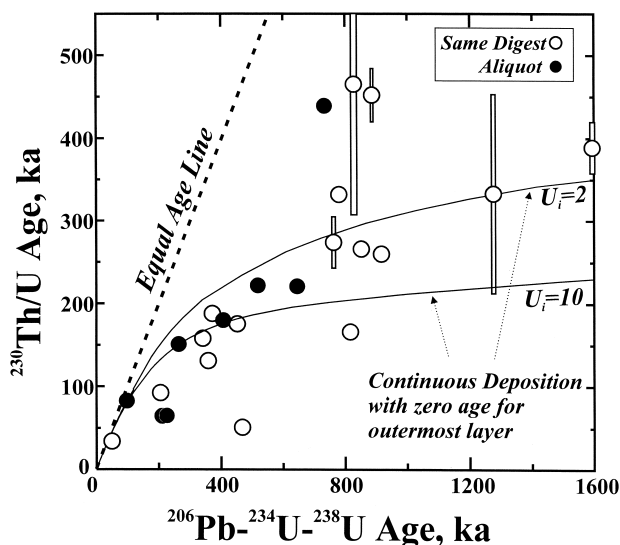


Fig. 8. A comparison between $^{230}\text{Th}/^{234}\text{U}$ ($T_{0/4}$) and $^{206}\text{Pb}/^{234}\text{U}$ ($T_{6/4}$) ages for subsamples of outermost opal collected from the same surface of fracture- and cavity-coating calcite–silica deposits. In all cases $T_{0/4}$ apparent ages are younger than $T_{6/4}$ ages. Curves are predictions of the continuous deposition model for different $^{234}\text{U}/^{238}\text{U}$ initial activity ratios ($U_i = 2$ and $U_i = 10$). Analyses were done either from different splits of a sample (aliquot) or from a single sample digest using mixed U–Th–Pb spike (same digest).

Mountain. On the basis of the combined U–Th–Pb dating, it seems that mineral deposition occurred very slowly over long periods of time. Interpreting the U–Pb geochronologic data within a continuous deposition framework suggests that secondary hydrogenic minerals were accumulating over much longer periods of time than is calculated from the models based on $^{230}\text{Th}/\text{U}$ or ^{14}C ages and an instantaneous deposition assumption. Therefore, the percolation fluxes responsible for mineral formation can be smaller because growth histories extend over longer time intervals. Also, because the combined U–Th–Pb dating results, as well as any other geochronologic data obtained at a similar sampling scale, are just average ages of multiage materials, rather than dates of rapid episodic growth of opal during a limited number of discrete depositional events, they cannot be directly correlated with the chronology of changes in surface climate conditions.

It is worth mentioning that the model of continuous deposition used here is just a simplified mathematical representation of an idealized process possible in the Yucca Mountain unsaturated zone environment. Actual depositional processes probably lie somewhere between the two extremes of discrete and continuous growth. Slow rates of deposition (mm/m.yr and slower) probably do occur over long periods of time. However, these rates are probably not constant, and they may be punctuated by at least short episodes of nondeposition. Nevertheless, a large number of thin, episodically deposited layers will approximate a continuous record of deposition. A zero-age, or even uniform age (for instance, last glacial maximum), for the outer mineral surface is probably also an unrealistic aspect of the continuous deposition model. The level of spatial resolution required to address the detailed growth, and by inference,

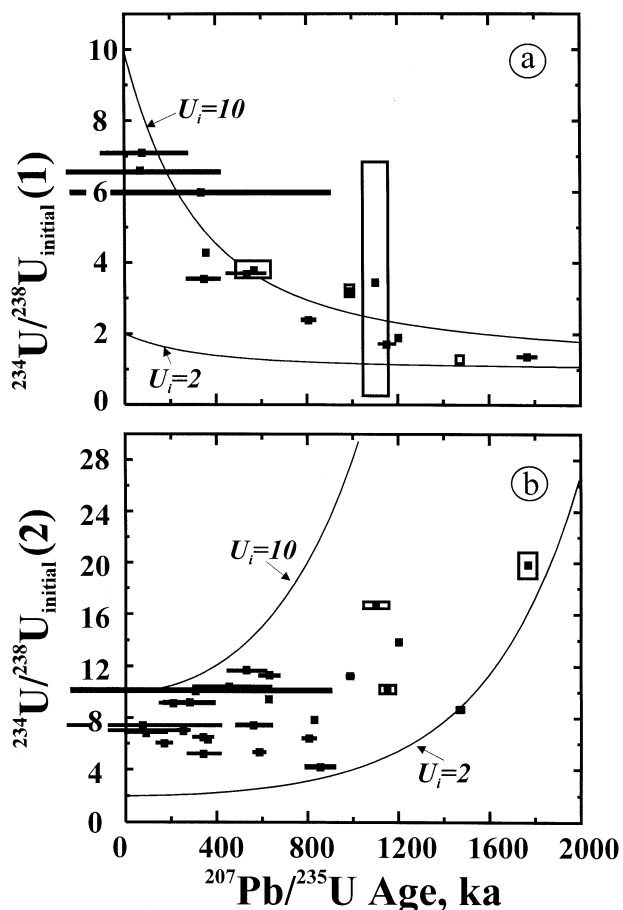


Fig. 9. Relations between $^{207}\text{Pb}/^{235}\text{U}$ ($T_{7/5}$) age and $^{234}\text{U}/^{238}\text{U}$ initial activity ratios (U_i) for Yucca Mountain opals. (a) U_i (1) calculated from the measured $^{234}\text{U}/^{238}\text{U}$ and $^{230}\text{Th}/^{238}\text{U}$ as shown in Fig. 3 and (b) U_i (2) calculated from the measured $^{234}\text{U}/^{238}\text{U}$ and $^{207}\text{Pb}^*/^{235}\text{U}$ as shown in Fig. 4b. Data are listed in Table 4. Curved lines are loci of apparent ages and $^{234}\text{U}/^{238}\text{U}$ initial activity ratios calculated for continuously deposited materials with $U_i = 2$ and $U_i = 10$.

percolation histories in the deep UZ at Yucca Mountain has yet to be attained.

6. CONCLUSIONS

The data presented in this paper illustrate that reliable geochronologic information can be obtained by combined U–Pb and U-series dating of Quaternary opal occurring in calcite–silica fracture and cavity coatings within Tertiary tuffs at Yucca Mountain. High U concentration, low abundances of common lead and initial ^{230}Th , and a considerable resistance of this material to short-lived interactions with reactive media with regard to loss of uranium and its daughter decay products (as demonstrated by laboratory experiments) are attractive attributes of opal as a mineral geochronometer.

Calculated U–Pb ages of the opals display strong reverse discordance and $^{207}\text{Pb}^*/^{206}\text{Pb}^*$ apparent ages are negative because of the excess of radiogenic $^{206}\text{Pb}^*$ derived from the elevated initial ^{234}U . The strong initial radioactive disequilibrium and young age of the opals allow data interpretation using

a new four-dimensional concordia diagram with $^{206}\text{Pb}^*/^{238}\text{U}$, $^{207}\text{Pb}^*/^{235}\text{U}$, $^{234}\text{U}/^{238}\text{U}$ activity, and $^{230}\text{Th}/^{238}\text{U}$ activity axes. Initial $^{234}\text{U}/^{238}\text{U}$ activity ratios typically between 2.6 and 11.8 and ages of 34.1 ± 0.6 ka to 1772 ± 40 ka have been calculated using the $^{230}\text{Th}/^{238}\text{U}$ – $^{234}\text{U}/^{238}\text{U}$, $^{206}\text{Pb}^*/^{238}\text{U}$ – $^{234}\text{U}/^{238}\text{U}$, $^{206}\text{Pb}^*/^{238}\text{U}$ – $^{230}\text{Th}/^{238}\text{U}$, and $^{207}\text{Pb}^*/^{235}\text{U}$ – $^{206}\text{Pb}^*/^{238}\text{U}$ projections. Use of the U–Pb technique to date these Quaternary opals significantly extends the age range beyond the limit of $^{230}\text{Th}/\text{U}$ dating method. Results show that selected fracture groundwater pathways in the unsaturated zone felsic tuffs of Yucca Mountain have been active throughout the Quaternary.

U–Th–Pb isotopic data are consistent with closed system radioactive decay, but conflict with common age interpretations based on assumed instantaneous formation of the dated opals. Aspects of instantaneous deposition most difficult to explain are discordant ages and $^{234}\text{U}/^{238}\text{U}$ initial ratios calculated from different Pb/U, $^{234}\text{U}/^{238}\text{U}$, and $^{230}\text{Th}/^{238}\text{U}$ ratios. The data instead support slow rates (mm/m.yr or less) of continuous mineral deposition and integration of multiage materials during sampling. U–Pb ages, which are systematically older than $^{230}\text{Th}/\text{U}$ ages, provide more accurate estimates of the average age of deposition for time-integrated mixed samples relative to $^{230}\text{Th}/\text{U}$ ages, because ages based on shorter-lived isotopes are nonlinearly biased to smaller values by younger mineral additions.

Acknowledgments—Loretta M. Kwak performed the chemical work for the U.S. Geological Survey laboratory part of this study and B. Podstawski provided mass-spectrometer maintenance at the Royal Ontario Museum, for which the authors are greatly appreciative. We gratefully acknowledge discussions with our colleagues on the Yucca Mountain Project, in particular Z. E. Peterman, B. D. Marshall, and J. F. Whelan, who provided both support and stimulation for these studies. F. Corfu, R. Mundil, W. Premo, J. Stuckless, and an unknown reviewer also made a number of valuable comments that improved the manuscript. The work was done in cooperation with the U.S. Department of Energy under Interagency Agreement No. DE-AI08-97NV12033.

REFERENCES

- Albarède F. (1995) *Introduction to Geochemical Modeling*. Cambridge University Press.
- Amelin Yu. V. and Zaitsev A. (1997) Precise U–Th–Pb chronology of carbonatites and phosphorites: Problems related to extreme elemental fractionation, and possible solution using multi-mineral approach. *Abstracts with Programs GAC/MAC Annual Meeting* **22**, A-2 (abstr.).
- Amelin Yu. V., Heaman L. M., Verkhogliad V. M., and Skobelev V. M. (1994) Geochronological constraints on the emplacement history of an anorthosite–rapakivi granite suite: U–Pb zircon and baddeleyite study of the Korosten complex, Ukraine. *Contrib. Mineral. Petrol.* **116**, 411–419.
- Barth S., Oberli F., and Meier M. (1994) Th–Pb versus U–Pb isotope systematics in allanite from co-genetic rhyolite and granodiorite: Implications for geochronology. *Earth Planet. Sci. Lett.* **124**, 149–159.
- Bateman H. (1910) Solution of a system of differential equations occurring in the theory of radio-active transformations. *Proc. Cambridge Phil. Soc.* **15**, 423–427.
- Bischoff J. L., Rosenbauer R. J., Moench A. F., and Ku T. L. (1995) U-series equations for uranium assimilation by fossil bones. *Radiochim. Acta* **69**, 127–135.
- Browne E. and Firestone R. (1986) *Table of Radioactive Isotopes*. John Wiley & Sons.
- Catchen G. L. (1984) Application of the equations of radioactive growth and decay to geochronological models and explicit solution of the equations by Laplace transformations. *Isot. Geosci.* **2**, 181–195.
- Cheng H., Edwards R. L., Murrell M. T., and Benjamin T. M. (1999) Uranium–thorium–protactinium dating systematics. *Geochim. Cosmochim. Acta* **62**, 3437–3452.
- Christiansen R. L., Lipman P. W., Carr W. J., Byers F. M. Jr., Orkild P. P., and Sargent K. A. (1977) Timber Mountain–Oasis Valley caldera complex of southern Nevada. *GSA Bull.* **88**, 943–959.
- De Bievre P., Lauer K. F., Le Duigou Y., Moret H., Muschenborn G., Spaepen J., Spagnol A., Vaninbrouck R., and Verdingh, V. (1971) The half-life of U-234. In *Proc. Intl. Conf. Chem. Nucl. Data, Measurement and Applications, Canterbury* (ed. M. L. Hurrell), p. 221–225. Inst. Civil Eng.
- Dickson B. L. and Wheller G. E. (1992) Uranium-series disequilibrium in exploration geology. In *Uranium-Series Disequilibrium: Applications to Earth, Marine, and Environmental Sciences, 2nd ed.* (ed. M. Ivanovich and R. S. Harmon), pp. 704–729. Clarendon Press.
- Edwards R. L., Chen J. H., and Wasserburg G. J. (1987) ^{238}U – ^{234}U – ^{230}Th – ^{232}Th systematics and the precise measurement of time over the past 500,000 years. *Earth Planet. Sci. Lett.* **81**, 175–192.
- Faure G. (1986) *Principles of Isotope Geology*. John Wiley & Sons.
- Gascoyne M. (1992) Geochemistry of the actinides and their daughters. In *Uranium-Series Disequilibrium: Applications to Earth, Marine, and Environmental Sciences, 2nd ed.* (ed. M. Ivanovich and R. S. Harmon), pp. 34–61. Clarendon Press.
- Ivanovich M. and Harmon R. S. (ed.) (1992) *Uranium-Series Disequilibrium: Applications to Earth, Marine, and Environmental Sciences, 2nd ed.* Clarendon Press.
- Jaffey A. H., Flynn K. F., Glendenin L. F., Bentley W. C., and Essling A. M. (1971) Precision measurements of half-lives and specific activities of ^{235}U and ^{238}U . *Phys. Rev.* **C4**, 1889–1906.
- Kaufman A. and Broecker W. S. (1965) Comparison of ^{230}Th and ^{14}C ages for carbonate materials from lakes Lahontan and Bonneville. *J. Geophys. Res.* **70**, 4039–4054.
- Krogh T. E. (1973) A low-contamination method for hydrothermal decomposition of zircon and extraction U and Pb for isotopic age determinations. *Geochim. Cosmochim. Acta* **37**, 485–494.
- Langmuir D. (1978) Uranium solution–mineral equilibria at low temperature with application to sedimentary ore deposits. *Geochim. Cosmochim. Acta* **42**, 547–569.
- Langmuir D. and Herman J. S. (1980) The mobility of thorium in natural waters at low temperatures. *Geochim. Cosmochim. Acta* **44**, 1753–1766.
- Lounsbury M. and Durham R. W. (1971) The alpha half-life of U-234. In *Proc. Intl. Conf. Chem. Nucl. Data, Measurement and Applications, Canterbury* (ed. M. L. Harrel), pp. 215–219. Inst. Civil Eng.
- Ludwig K. R. (1977) Effect of initial radioactive-daughter disequilibrium on U–Pb isotope apparent ages of young minerals. *J. Res. U.S. Geol. Survey* **5**, 663–667.
- Ludwig K. R. (1988) *PBDAT for MS-DOS. A Computer Program for IBM PC Compatibles for Processing Raw Pb–U–Th Isotope Data*. USGS Open-File Report 88-0542.
- Ludwig K. R. (1997) *ISOPLOT: A Plotting and Regression Program for Radiogenic-Isotope Data; Version 2.95 (July 1997 rev.)*. USGS Open-File Report 91-445.
- Ludwig K. R., Lindsey D. A., Zielinski R. A., and Simmons K. R. (1980) U–Pb ages of uraniumiferous opal and implication for the history of beryllium, fluorine, and uranium mineralization at Spor Mountain, Utah. *Earth Planet. Sci. Lett.* **46**, 221–232.
- Ludwig K. R., Wallace A. R., and Simmons K. R. (1985) The Schwarzwald uranium deposit. II: Age of uranium mineralization and lead isotope constraints on genesis. *Econ. Geol.* **80**, 1858–1871.
- Mattinson J. M. (1973) Anomalous isotopic composition of lead in young zircons. *Carnegie Inst. Washington Yearbook* **72**, 613–616.
- Meadows J. W., Armani R. J., Callis E. L., and Essling A. M. (1980) Half-life of ^{230}Th . *Phys. Rev.* **C22**, 750–754.
- Meijer A. (1992) A strategy for the derivation and use of sorption coefficients in performance assessment calculations for the Yucca Mountain site. *Proceedings of the DOE/Yucca Mountain Site Characterization Project Radionuclide Adsorption Workshop at Los Alamos National Laboratory*, September 11–12, 1990. Canepa, J. A., ed. LA-12325-C. Los Alamos, New Mexico: Los Alamos National Laboratory. ACC: NNA.19920421.0117.

- Neymark L. A. and Paces J. B. (1996) Mixed isotopic ages as a consequence of very slow rates of deposition in Quaternary subsurface fracture coatings, GSA Annual Meeting, October 28–31, Denver, Colorado, *Abstracts with Programs*, 28, N7, p. A-139 (abstr.).
- Neymark L. A. and Paces J. B. (2000) Consequences of slow growth for $^{230}\text{Th}/\text{U}$ dating of Quaternary opals, Yucca Mountain, Nevada, USA. *Chem. Geol.* **164**, 143–160.
- Neymark L. A., Marshall B. D., Kwak L., Futa K., and Mahan S. A. (1995) *Geochemical and Pb, Sr, and O Isotopic Study of the Tiva Canyon Tuff and Topopah Spring Tuff, Yucca Mountain, Nye County, Nevada*. USGS Open-File Report 95-134.
- Neymark L. A., Amelin Y. V., Paces J. B., and Peterman Z. E. (1998a) U–Pb age evidence for long-term stability of the unsaturated zone, Yucca Mountain, Nevada. *Proc., Intl. High-Level Rad. Waste Manag. Conf. Las Vegas, NV, May 11–14, 1998*, pp. 85–87. Amer. Nucl. Soc.
- Neymark L. A., Paces J. B., and Amelin Y. V. (1998b) Neogene to Quaternary U–Th–Pb geochronology using opal, Yucca Mountain, Nevada, USA. *Mineral. Mag.* **62A**, 1077–1078 (abstr.).
- Oberli F., Meier M., Berger A., Rosenberg C., and Giere R. (1996) $^{230}\text{Th}/^{238}\text{U}$ disequilibrium systematics in U–Th–Pb dating: Nuisance or powerful tool in geochronometry? Sixth Annual V. M. Goldschmidt Conference, 31 March–4 April, 1996, Heidelberg, Germany. *J. Conf. Abstr.* **1**, 439 (abstr.).
- Olley J. M., Roberts R. G., and Murray A. S. (1997) A novel method for determining residence times of river and lake sediments based on disequilibrium in the thorium decay series. *Water Resour. Res.* **33**, 1319–1326.
- Ostholts A. (1995) Thorium sorption on amorphous silica. *Geochim. Cosmochim. Acta* **59**, 1235–1249.
- Paces J. B., Neymark L. A., Kwak L. M., and Peterman Z. E. (1996) U-series dating of secondary minerals as a tool for estimating paleo water flux through a thick unsaturated zone, Yucca Mountain, NV, GSA annual meeting, October 28–31, Denver, Colorado, *Abstracts with Programs*, p. A-139–140 (abstr.).
- Paces J. B., Neymark L. A., Marshall B. D., Whelan J. F., and Peterman Z. E. (1998a) Inferences for Yucca Mountain unsaturated zone hydrology from secondary minerals. *Proc., Intl. High-Level Rad. Waste Manag. Conf., Las Vegas, NV, May 11–14, 1998*, pp. 36–39. Amer. Nucl. Soc.
- Paces J. B., Ludwig K. R., Peterman Z. E., Neymark L. A., and Kenneally J. M. (1998b) Anomalous ground-water $^{234}\text{U}/^{238}\text{U}$ beneath Yucca Mountain: Evidence of local recharge? *Proc., Intl. High-Level Rad. Waste Manag. Conf., Las Vegas, NV, May 11–14, 1998*, pp. 185–188. Amer. Nucl. Soc.
- Parrish R. R. (1990) U–Pb dating of monazite and its application to geological problems. *Can. J. Earth Sci.* **27**, 1431–1450.
- Richards D. A., Bottrell S. H., Cliff R. A., Stroehle K., and Rowe P. J. (1998) U–Pb dating of a speleothem of Quaternary age. *Geochim. Cosmochim. Acta* **62**, 3683–3688.
- Sawyer D. A., Fleck R. J., Lanphere M. A., Warren R. G., and Broxton D. E. (1994) Episodic volcanism in the Miocene southwest Nevada volcanic field—stratigraphic revisions, $^{40}\text{Ar}/^{39}\text{Ar}$ geochronologic framework, and implications for magmatic evolution. *GSA Bull.* **106**, 1304–1318.
- Schärer U. (1984) The effect of initial ^{230}Th disequilibrium on young U–Pb ages: The Makalu case, Himalaya. *Earth Planet. Sci. Lett.* **67**, 191–204.
- Scott R. D., MacKenzie A. B., and Alexander W. R. (1992) The interpretation of ^{238}U – ^{234}U – ^{230}Th – ^{226}Ra disequilibria produced by rock–water interactions. *J. Geochem. Explor.* **45**, 323–343.
- Tatsumoto M. (1966) Isotopic composition of lead in volcanic rocks from Hawaii, Iwo Jima, and Japan. *J. Geophys. Res.* **71**, 1721–1733.
- U.S. Department of Energy. (1988) *Site Characterization Plan, Yucca Mountain Site, Nevada Research and Development Area, Nevada*. U.S. Dept. Energy Report DOE/RW-0199, 8 volumes.
- Wendt I. and Carl C. (1985) U/Pb dating of discordant 0.1 Ma old secondary U minerals. *Earth Planet. Sci. Lett.* **73**, 278–284.
- Wiedenbeck M., Allé P., Corfu F., Griffin W. L., Meier M., Oberli F., Von Quadt A., Roddick J. C., and Spiegel W. (1995) Three natural standards for U–Th–Pb, Lu–Hf, trace element and REE analyses, *Geostandards Newsl.* **19**, 1–23.
- Winograd I. J. (1981) Radioactive waste disposal in thick unsaturated zones. *Science* **212**, 1457–1464.
- Zartman R. E. and Kwak L. M. (1993) *Preliminary Study of Lead Isotopes in the Carbonate–Silica Veins of Trench-14, Yucca Mountain*. USGS Open-File Report 93-690.
- Zielinski R. A. (1982) Uraniferous opal, Virgin Valley, Nevada: Conditions of formation and implications for uranium exploration. *J. Geochem. Explor.* **16**, 197–216.

APPENDIX 1. EQUATIONS FOR U–PB AGE CALCULATIONS

Ages are calculated from $^{206}\text{Pb}^*/^{238}\text{U}$ and $^{207}\text{Pb}^*/^{235}\text{U}$ ratios using the following equations (Faure, 1986):

$$\left(\frac{^{207}\text{Pb}^*}{^{235}\text{U}}\right)_t = e^{\lambda_{235}t} - 1, \quad (\text{A1})$$

and

$$\left(\frac{^{206}\text{Pb}^*}{^{238}\text{U}}\right)_t = e^{\lambda_{238}t} - 1, \quad (\text{A2})$$

where t is age of formation, λ_{235} and λ_{238} are decay constants of ^{235}U and ^{238}U , respectively, and $^{206}\text{Pb}^*$ and $^{207}\text{Pb}^*$ are radiogenic Pb isotope abundances.

Eqns. A1 and A2 are accurate only for the case of initial secular radioactive equilibrium in uranium radioactive decay chains, that is, they assume that activities of all radioactive intermediate daughter isotopes were equal to the activity of their parent isotope at the moment of formation of the analyzed rock or mineral. Using equations that take into account initial radioactive disequilibria of the uranium daughters is highly desirable in solving problems of dating very young minerals. The more general form of the apparent age equations for a closed system older than 1000 yr is given by the following equations (Ludwig, 1977; Wendt and Carl, 1985), which consider only daughters with half-lives longer than 1 yr:

$$\left(\frac{^{207}\text{Pb}^*}{^{235}\text{U}}\right)_t = e^{\lambda_{235}t} (B_1 e^{-\lambda_{235}t} + B_2 e^{-\lambda_{231}t} + B_3 e^{-\lambda_{227}t} + 1) \quad (\text{A3})$$

$$\left(\frac{^{206}\text{Pb}^*}{^{238}\text{U}}\right)_{t(\text{total})} = R_1 (\text{from } ^{234}\text{U}) \quad (\text{A4})$$

$$R_1 = e^{\lambda_{238}t} (C_1 e^{-\lambda_{238}t} + C_2 e^{-\lambda_{234}t} + C_3 e^{-\lambda_{230}t} + C_4 e^{-\lambda_{226}t} + C_5 e^{-\lambda_{210}t} + 1) \quad (\text{A5})$$

$$R_2 = \frac{\lambda_{238}}{\lambda_{234}} e^{\lambda_{238}t} \left(\frac{^{234}\text{U}}{^{238}\text{U}}\right)_{A_0} (D_1 e^{-\lambda_{234}t} + D_2 e^{-\lambda_{230}t} + D_3 e^{-\lambda_{226}t} + D_4 e^{-\lambda_{210}t} + 1), \quad (\text{A6})$$

where λ_n is a decay constant of isotope n (^{235}U , ^{231}Pa , ^{227}Ac , ^{238}U , ^{234}U , ^{230}Th , ^{226}Ra , and ^{210}Pb), t = age, and $(^{234}\text{U}/^{238}\text{U})_{A_0}$ is the initial activity ratio of $^{234}\text{U}/^{238}\text{U}$. B_1 , C_1 , and D_1 are the Bateman's coefficients (Bateman, 1910) for a chain of multiple successive decays given by equation:

$$B_i = \prod_{i=1}^{n-1} \lambda_i / \prod_{j=1}^n (\lambda_j - \lambda_i), \quad (\text{A7})$$

where $i = 1, 2, 3, \dots, n$; $j \neq i$; n = number of isotopes in the decay chain. In this case the i and j values for Eqn. A7 correspond to the order of the daughter isotope in the ^{235}U or ^{238}U decay chain. The decay constants for stable decay products ^{207}Pb and ^{206}Pb are $\lambda_{207} = \lambda_{206} =$

0. Thus, the coefficients are: $B_1 = \frac{-\lambda_{231} \lambda_{227}}{(\lambda_{231} - \lambda_{235})(\lambda_{227} - \lambda_{235})}$,
 $B_2 = \frac{-\lambda_{235} \lambda_{227}}{(\lambda_{235} - \lambda_{231})(\lambda_{227} - \lambda_{231})}$, $B_3 = \frac{-\lambda_{235} \lambda_{231}}{(\lambda_{235} - \lambda_{227})(\lambda_{231} - \lambda_{227})}$,
 and so on. Eqns. A3 through A6 assume negligible initial ^{231}Pa , ^{227}Ac , ^{230}Th , ^{226}Ra , ^{210}Pb , ^{207}Pb , and ^{206}Pb .

For samples younger than 1–2 Ma, having measurable amounts of excess ^{234}U (today's activity ratio $(^{234}\text{U}/^{238}\text{U})_{\text{At}} > 1$) two more equations are needed to describe the temporal evolution of $^{234}\text{U}/^{238}\text{U}$ and $^{230}\text{Th}/^{238}\text{U}$ activity ratios (Ivanovich and Harmon, 1992; Albarède, 1995):

$$\left(\frac{^{234}\text{U}}{^{238}\text{U}}\right)_{\text{At}} = \left[\left(\frac{^{234}\text{U}}{^{238}\text{U}}\right)_{\text{A0}} - 1 \right] \cdot e^{-\lambda_{234}t} + 1; \quad (\text{A8})$$

$$\left(\frac{^{230}\text{Th}}{^{238}\text{U}}\right)_{\text{At}} = \left(1 - e^{-\lambda_{230}t} + \frac{\lambda_{230}}{\lambda_{230} - \lambda_{234}} \cdot \left[\left(\frac{^{234}\text{U}}{^{238}\text{U}}\right)_{\text{A0}} - 1 \right] \cdot (e^{-\lambda_{234}t} - e^{-\lambda_{230}t}) \right), \quad (\text{A9})$$

where indexes At and A0 correspond to measured and initial activity ratios, respectively.

A combination of Eqns. A4, A8, and A9 offers the possibility of creating two new concordia plots $^{234}\text{U}/^{238}\text{U}_{\text{activity}}$ vs. $^{206}\text{Pb}^*/^{238}\text{U}$ and $^{230}\text{Th}/^{238}\text{U}_{\text{activity}}$ vs. $^{206}\text{Pb}^*/^{238}\text{U}$. Isolation of $(^{234}\text{U}/^{238}\text{U})_{\text{A0}}$ from Eqn. A8 and its substitution to Eqn. A6 provides solutions for both age (t) and $^{234}\text{U}/^{238}\text{U}_{\text{initial}}$ activity ratio using measured values of $^{234}\text{U}/^{238}\text{U}$ and $^{206}\text{Pb}^*/^{238}\text{U}$. Using the same approach and isolating $(^{234}\text{U}/^{238}\text{U})_{\text{A0}}$ from Eqn. A9, age and uranium initial activity ratio can be calculated from measured values of $^{230}\text{Th}/^{238}\text{U}_{\text{activity}}$ and $^{206}\text{Pb}^*/^{238}\text{U}$. Solutions for t and $(^{234}\text{U}/^{238}\text{U})_{\text{A0}}$ are presented in Table 4. Errors were propagated assuming their statistical independence from the general equation:

$$\sigma_{f(x_1, \dots, x_n)}^2 = \sum_{i=1}^n \left(\frac{\partial f}{\partial x_i} \right)^2 \sigma_{x_i}^2. \quad (\text{A10})$$